

# 1 Subunit-selective proteasome activity profiling uncovers uncoupled 2 proteasome subunit activities during bacterial infections

3

4 Johana C. Misas-Villamil<sup>1,2</sup>, Aranka M. van der Burgh<sup>1,8</sup>, Friederike Grosse-Holz<sup>7</sup>, Marcel Bach-  
5 Pages<sup>7</sup>, Judit Kovács<sup>1,6</sup>, Farnusch Kaschani<sup>3</sup>, Sören Schilasky<sup>1</sup>, Asif Emron Khan Emon<sup>1,4</sup>, Mark  
6 Ruben<sup>5</sup>, Markus Kaiser<sup>3</sup>, Hermen S. Overkleeft<sup>5</sup>, and Renier A. L. van der Hoorn<sup>1,7\*</sup>

7

8 <sup>1</sup> The Plant Chemetics Laboratory, Max Planck Institute for Plant Breeding Research, Carl-von-Linné  
9 Weg 10, 50829 Cologne, Germany

10 <sup>2</sup> Botanical Institute and Cluster of Excellence on Plant Sciences, University of Cologne, 50674  
11 Cologne, Germany

12 <sup>3</sup> Chemical Biology, Universität Duisburg-Essen, Zentrum für Medizinische Biotechnologie, Fakultät  
13 für Biologie, Universitätsstr. 2, 45117 Essen, Germany

14 <sup>4</sup> Current address: Bonn-Aachen International Center for IT, University of Bonn, Dahlmannstrasse 2,  
15 53113 Bonn, Germany

16 <sup>5</sup> Institute of Chemistry and Netherlands Proteomics Centre, Gorlaeus Laboratories, 2333 CC Leiden,  
17 The Netherlands

18 <sup>6</sup> Department of Plant Biology, University of Szeged, Szeged, Hungary

19 <sup>7</sup> The Plant Chemetics Laboratory, Department of Plant Sciences, University of Oxford, South Parks  
20 Lane OX1 3RB Oxford, United Kingdom

21 <sup>8</sup> Current address: Laboratory for Phytopathology, Wageningen University, Droevendaalsesteeg 1,  
22 6708 PB Wageningen, The Netherlands.

23

24 \*, for correspondence: [renier.vanderhoorn@plants.ox.ac.uk](mailto:renier.vanderhoorn@plants.ox.ac.uk)

25

26 **Keywords:** catalytic subunit; core protease; *Arabidopsis thaliana*; *Nicotiana benthamiana*; Activity-  
27 based protein profiling; proteasome manipulation.

28

29 **Running head:** Subunit-selective proteasome activity profiling

30

31 **Significances Statement:** Proteasome activity profiling with subunit-selective fluorescent probes is a  
32 robust way to display activities of  $\beta 1$  and  $\beta 5$  activities in any plant species. We validate these next  
33 generation tools and use it to uncover that  $\beta 1$  and  $\beta 5$  activities are uncoupled upon infection by  
34 virulent bacteria.

35

36 **SUMMARY**

37 **The proteasome is a nuclear - cytoplasmic proteolytic complex involved in nearly all regulatory**  
38 **pathways in plant cells. The three different catalytic activities of the proteasome can have**  
39 **different functions but tools to monitor and control these subunits selectively are not yet**  
40 **available in plant science. Here, we introduce subunit-selective inhibitors and dual-color**  
41 **fluorescent activity-based probes for studying two of the three active catalytic subunits of the**  
42 **plant proteasome. We validate these tools in two model plants and use this to study the**  
43 **proteasome during plant-microbe interactions. Our data reveals that *Nicotiana benthamiana***  
44 **incorporates two different paralogs of each catalytic subunit into active proteasomes.**  
45 **Interestingly, both  $\beta 1$  and  $\beta 5$  activities are significantly increased upon infection with pathogenic**  
46 ***Pseudomonas syringae* pv. *tomato* DC3000 lacking hopQ1-1 (PtoDC3000( $\Delta$ hQ)) whilst the**  
47 **activity profile of the  $\beta 1$  subunit changes. Infection with wild-type PtoDC3000 causes**  
48 **proteasome activities that range from strongly induced  $\beta 1$  and  $\beta 5$  activities to strongly**  
49 **suppressed  $\beta 5$  activities, revealing that  $\beta 1$  and  $\beta 5$  activities can be uncoupled during bacterial**  
50 **infection. These selective probes and inhibitors are now available to the plant science community**  
51 **and can be widely and easily applied to study the activity and role of the different catalytic**  
52 **subunits of the proteasome in different plant species.**

53

## 54 **INTRODUCTION**

55 The ubiquitin proteasome pathway is responsible for the selective degradation of proteins in the cell  
56 regulating numerous cellular and physiological functions. The proteasome is a multi-subunit, ATP-  
57 dependent proteolytic complex consisting of a 20S core particle (CP) and a 19S regulatory particle  
58 (RP) (Groll et al., 1997). The CP is ubiquitin and ATP independent, and consists of four stacked rings  
59 forming a barrel. The inner two rings of the barrel consist of  $\beta$  subunits and these are flanked by two  
60 rings of  $\alpha$  subunits (Kurepa and Smalle, 2008a). Each ring consists of seven subunits. The catalytic  
61 subunits responsible for peptide cleavage are located in the  $\beta$  rings and have an active site N-terminal  
62 Threonine (Thr). The catalytic  $\beta$  subunits have different proteolytic activities:  $\beta 1$  has caspase-like  
63 activity,  $\beta 2$  trypsin-like activity and  $\beta 5$  chymotrypsin-like activity (Dick et al., 1998).

64 In addition to its crucial role in plant hormone signaling, the ubiquitin proteasome pathway  
65 has received attention in the plant pathogen field because several pathogens target this system. The  
66 proteasome acts as a hub in various immune signalling cascades, and is therefore an obvious target for  
67 pathogens (Üstün et al., 2016). Pathogen-derived effectors were found to interact with components of  
68 the ubiquitin proteasome system such as E3-ligases, F-box proteins and SUMO de-conjugation  
69 enzymes (Banfield et al., 2015). These effectors interfere in vesicle trafficking or promote  
70 transcription factor degradation. Some of these bacterial effectors act by inhibiting the proteasome.  
71 For instance, the XopJ effector produced by *Xanthomonas campestris* pv. *vesicatoria* and the HopZ4  
72 effector from *Pseudomonas syringae* pv. *lachrymans* interact with the RPT6 subunit of the 19S  
73 regulatory particle, suppressing the activity of the proteasome and repressing salicylic acid (SA)

74 mediated responses (Üstün et al., 2013; 2014). In addition, the non-ribosomal polypeptide Syringolin  
75 A (SylA) secreted by *Pseudomonas syringae* pv. *syringae* also targets the proteasome (Groll et al.,  
76 2008), in this case by covalently inhibiting  $\beta 2$  and  $\beta 5$  subunits of the plant proteasome (Kolodziejek et  
77 al. 2011). SylA facilitates opening of stomata and promotes bacterial colonization from wound sites  
78 (Misas-Villamil et al., 2013; Schellenberg et al., 2010).

79         So far, the plant proteasome could not be sufficiently investigated due to technical limitations  
80 and lack of suitable approaches. First, reverse genetic approaches are challenging since mutations in  
81 CP subunits usually cause severe pleiotropic defects or even lethality (Kurepa and Smalle, 2008a).  
82 Roles of the different CP subunits are also impossible to study using a knockout approach since the CP  
83 requires integrity for its function. Second, a number of proteasome subunits are modified post-  
84 translationally, e.g. by proteolytic processing, acetylation and ubiquitylation (Book et al., 2010). Third,  
85 the proteasome is a versatile complex in which substrate specificities can be changed, depending on  
86 the assembly of the different subunits. The most notable example is the immunoproteasome in  
87 mammals in which constitutive subunits of the CP are replaced by inducible subunits (Aki et al.,  
88 1994). The recently discovered replacement of  $\alpha 3$  by  $\alpha 4$  in human proteasomes is another example of  
89 alternative proteasomes (Padmanabhan et al., 2016). Although there is no evidence that plants have an  
90 alternative proteasome, plant genomes carry multiple genes for nearly each subunit (Yang et al., 2004)  
91 and the proteasome in *Arabidopsis* is assembled with paralogous pairs for most subunits (Book et al.,  
92 2010). Remarkably, tobacco genes encoding  $\beta 1$ ,  $\alpha 3$  and  $\alpha 6$  subunits are transcriptionally upregulated  
93 after treatment with the elicitor cryptogein (Suty et al., 2003) indicating that plants might assemble  
94 inducible alternative proteasomes.

95         The activity of the proteasome subunits can be studied using fluorogenic substrates, which  
96 require the isolation and purification of the proteasome, a very tedious and laborious method only  
97 applicable on certain soft plant tissues (Yang et al., 2004; Book et al., 2010). We previously  
98 introduced activity-based protein profiling (ABPP) to monitor the activity of the plant proteasome (Gu  
99 et al., 2010). ABPP relies on the use of small molecule chemical probes that are composed of a  
100 reactive group, a linker and a reporter tag that can be biotin or fluorescent to facilitate protein  
101 purification and detection, respectively (Cravatt et al., 2008). These chemical probes react with the  
102 active site of enzymes, resulting in a covalent and often irreversible labeling, which facilitates the  
103 detection, purification and identification of those labeled proteins. Labeling reflects protein activity  
104 rather than abundance because the probes only react when the active site is available and reactive and  
105 many enzymes are regulated by changes in the availability and reactivity of the active site. So far we  
106 have introduced over 40 activity-based probes into plant science to monitor e.g. Cys proteases,  
107 glycosidases, subtilases, acyltransferases and glutathione transferases, and many of these probes are  
108 widely used in plant science (Morimoto and Van der Hoorn, 2016). DCG-04, for instance, is a probe  
109 for papain-like Cys proteases (Greenbaum et al., 2000; Van der Hoorn et al., 2004) that has been  
110 instrumental for the discovery of pathogen-derived inhibitors (Rooney et al., 2005; Tian et al., 2007;

111 Shabab et al., 2008; Van Esse et al., 2008; Song et al., 2009; Kaschani et al., 2010; Lozano-Torres et  
112 al., 2012; Mueller et al., 2013), deciphering protease-inhibitor arms-races and effector adaptation upon  
113 a host jump (Hörger et al., 2012; Dong et al., 2014), and identifying senescence-associated proteases  
114 (Martinez et al., 2007; Carrion et al., 2013; Porret et al., 2015). Likewise, proteasome probes have  
115 been used to describe post-translational activation of the proteasome during salicylic acid signaling  
116 (Gu et al., 2010), the selective suppression of the nuclear proteasome by bacterial phytotoxin  
117 Syringolin A (SylA, Kolodziejek et al., 2011; Misas-Villamil et al., 2013); and the regulation of the  
118 proteasome by NAC transcription factor RPX (Nguyen et al., 2013), the validation and availability of  
119 next generation chemical probes will underpin exciting scientific discoveries.

120 The activity of the three catalytic subunits of the Arabidopsis proteasome can be easily  
121 distinguished using ABPP since these subunits have different molecular weight (MW) (Gu et al.,  
122 2010; Kolodziejek et al., 2011). In other plants, however, the MW of these different subunits can  
123 overlap and multiple subunit genes can cause additional signals that are difficult to annotate (Gu,  
124 2010). In the model plant *Nicotiana benthamiana*, for instance, all three different catalytic subunits  
125 were detected in a single band (Misas-Villamil et al., 2013). Here, we describe subunit-specific  
126 labeling for two catalytic subunits. By using these next generation probes we are able to display  
127 activities of  $\beta 1$  and  $\beta 5$  catalytic subunits in *N. benthamiana*, revealing that activity of these subunits  
128 independently change upon bacterial infection.

129

## 130 RESULTS

131 *LW124 and MVB127 are selective probes for the  $\beta 1$  and  $\beta 5$  catalytic subunits*

132 We have previously used MVB072 (**Figure 1a**), a probe that labels all three catalytic subunits of the  
133 plant proteasome (Kolodziejek et al., 2011). Labeling of Arabidopsis leaf extracts with MVB072  
134 results in three signals representing  $\beta 2$  (top band 1),  $\beta 5$  (middle band 2) and  $\beta 1$  (bottom band 3)  
135 (**Figure 1b**, Kolodziejek et al., 2011). We also have previously introduced a rhodamine-tagged SylA  
136 (RhSylA, **Figure 1a**) which preferentially labels  $\beta 2$  (top band 6), and  $\beta 5$  (bottom band 7) (**Figure 1b**,  
137 Kolodziejek et al., 2011).

138 Here we introduce two next generation probes for labeling of specific proteasome catalytic  
139 subunits. LW124 contains an epoxyketone reactive group, the tetrapeptide Ala-Pro-Nle-Leu and a  
140 bodipy Cy2 fluorescent group (**Figure 1a**, Li et al., 2013). MVB127 has a vinyl sulphone (VS)  
141 reactive group, a MeTyr-Phe-Ile tripeptide and a bodipy Cy2 fluorescent group with an azide group  
142 that can be used for click chemistry reactions (**Figure 1a**, Li et al., 2013). In contrast to MVB072  
143 labeling, which in Arabidopsis results in three signals, we detect only one signal for LW124 at 26 kDa  
144 (**Figure 1b**, band 4), and one signal for MVB127 at ca. 27 kDa (**Figure 1b**, band 5). No strong signals  
145 appear in the remainder of the gels (Supplemental **Figure S1**). All signals are caused by proteasome  
146 labeling since they are suppressed upon pre-incubation with the selective proteasome inhibitor  
147 epoxomicin (Supplemental **Figure S2**).

148 Because LW124 carries a different fluorophore, we tested if these probes can be mixed and  
149 used in co-labeling experiments. Co-labeling by adding two probes at the same time and with the same  
150 concentration to Arabidopsis leaf extracts indeed shows specific signals for both probes (**Figure 1c**).  
151 The bottom signal (band 3,  $\beta 1$ ) of MVB072 is suppressed upon co-labeling with LW124 (**Figure 1c**,  
152 lane 4), indicating that LW124 targets  $\beta 1$  of the Arabidopsis proteasome. The overlay shows that the  
153  $\beta 1$ -LW124 conjugate (band 4) migrates slightly faster in the protein gel than the  $\beta 1$ -MVB072  
154 conjugate (band 3), consistent with the different MW of the two probes (**Figure 1b** and **1c**, lanes 1 and  
155 2). A suppression of labeling cannot be observed upon co-labeling of MVB072 with MVB127 since  
156 they carry the same fluorophore (**Figure 1c**, lane 5). Co-labeling of LW124 with MVB127 results in  
157 two signals (**Figure 1c**, top two panels, lane 6), indicating that these probes label different subunits.  
158 However, the MVB127 signal (band 5) is suppressed upon colabeling with LW124 (**Figure 1c**, lanes 3  
159 and 6). By contrast, labeling by LW124 (band 4) seems unaffected upon co-labeling with MVB127  
160 (**Figure 1c**, lanes 2 and 6).

161 To confirm that LW124 and MVB127 are specific probes for one proteasome catalytic  
162 subunit, we pre-incubated the samples with subunit-specific proteasome inhibitors that have been  
163 validated on mammalian proteasomes. N3 $\beta 1$  is an epoxyketone inhibitor that targets the  $\beta 1$  catalytic  
164 subunit, whereas N3 $\beta 5$  is a vinyl sulphone inhibitor of the  $\beta 5$  catalytic subunit (**Figure 2a**, Verdoes et  
165 al., 2010). Notably, these are non-fluorescent versions of the probes since the peptide and reactive  
166 group (warhead) of N3 $\beta 1$  is identical to that of LW124 and the warhead of N3 $\beta 5$  is identical to that of  
167 MVB127 (**Figures 1a** and **2a**). Pre-incubation with N3 $\beta 1$  suppresses labeling of only the bottom band  
168 3 in the MVB072 labeling profile, confirming that this inhibitor is selective for the  $\beta 1$  subunit (**Figure**  
169 **2b**, lane 2). By contrast, pre-incubation with N3 $\beta 5$  suppresses MVB072 labeling of the middle band 2,  
170 confirming selectivity for  $\beta 5$  (**Figure 2b**, lane 3).

171 Having verified the selectivity of N3 $\beta 1$  and N3 $\beta 5$ , we tested if LW124 and MVB127 labeling  
172 can be suppressed by the respective subunit-selective inhibitor. N3 $\beta 1$  suppresses labeling of LW124  
173 (**Figure 2b**, lanes 5 and 8), confirming that LW124 targets  $\beta 1$ , consistent with the structural similarity  
174 of LW124 with N3 $\beta 1$  (**Figures 1a** and **2a**). Importantly, the suppression of MVB127 labeling by N3 $\beta 5$   
175 (**Figure 2b**, lanes 6 and 12) shows that MVB127 targets  $\beta 5$ , consistent with the structural similarity of  
176 MVB127 with N3 $\beta 5$  (**Figures 1a** and **2a**). The  $\beta 5$ -MVB127 conjugate (band 5) migrates slightly faster  
177 in the protein gel than the  $\beta 5$ -MVB072 conjugate (band 2), consistent with the different MW of the  
178 two probes (**Figures 1b** and **1c**, lanes 1 & 3, and **2b**, lanes 1 & 4). Importantly, pre-incubation of  
179 N3 $\beta 1$  or N3 $\beta 5$  in the reciprocal combinations with the probes, did only slightly reduce MVB127 and  
180 LW124 labeling, respectively (**Figure 2b**, lanes 5, 6, 9, and 11), indicating that both inhibitors and  
181 probes are specific for their targets. Taken together these data show that LW124 and MVB127 are  
182 selective probes for  $\beta 1$  and  $\beta 5$  catalytic subunits, respectively.

183

184 *Specific labeling of the  $\beta 2$  catalytic subunit*

185 Having established selective labeling of the  $\beta 1$  and  $\beta 5$  catalytic subunits, we next developed a method  
186 to monitor  $\beta 2$ . We previously found that RhSylA targets the proteasome subunits  $\beta 2$  and  $\beta 5$  at short  
187 labeling times (Kolodziejek et al., 2011). Taking advantage of this feature we tested if inhibition of the  
188  $\beta 5$  proteasome subunit using N3 $\beta 5$  together with short labeling by RhSylA will result in specific  
189 labeling of  $\beta 2$ . We therefore pre-incubated Arabidopsis leaf extracts with various concentrations of  
190 N3 $\beta 5$  and labeled for 30 min with 0.5  $\mu\text{M}$  RhSylA. Increasing N3 $\beta 5$  concentrations up to 5  $\mu\text{M}$  N3 $\beta 5$   
191 reduces  $\beta 5$  labeling (**Figures 3a** and **3b**).  $\beta 5$  labeling remains unaltered at higher N3 $\beta 5$  concentrations  
192 (**Figures 3a** and **3b**) indicating that  $\beta 5$  subunit is saturated by N3 $\beta 5$ . Signal intensities derived from  $\beta 1$   
193 and  $\beta 5$  at 5  $\mu\text{M}$  N3 $\beta 5$  are very faint in comparison to the  $\beta 2$  signal, which remains unaffected (**Figure**  
194 **3b**). This data demonstrates that RhSylA labeling in the presence of 5  $\mu\text{M}$  N3 $\beta 5$  is a suitable approach  
195 to monitor labeling of  $\beta 2$ .

196

197 *Subunit-specific probes display multiple  $\beta 1$  signals in *N. benthamiana**

198 *N. benthamiana* is increasingly used as a model plant to study protein regulation and localization upon  
199 transient expression. Additionally, *N. benthamiana* can be infected by a range of different pathogens,  
200 which makes this species ideal to unravel plant defense (Goodin et al., 2008). Labeling of *N.*  
201 *benthamiana* leaf extracts with MVB072 results in two signals: one strong signal at 28 kDa and one  
202 faint signal at ca. 27 kDa (**Figure 4a**, lane 1, bands 1 and 2, Misas-Villamil et al., 2013). MS analysis  
203 of the MVB072-labeled proteins representing the major signal revealed that it contains  $\beta 1$ ,  $\beta 2$  and  $\beta 5$   
204 subunits (Misas-Villamil et al., 2013). Thus, in contrast to Arabidopsis where the three catalytic  
205 subunits cause three distinct signals, the *N. benthamiana* proteasome subunits cannot be distinguished  
206 by MVB072 labeling because the signals overlap.

207 To monitor the catalytic subunits of the *N. benthamiana* proteasome, we tested the subunit-  
208 selective probes. Surprisingly, LW124 labeling displays two 27 kDa signals, indicating that there  
209 might be two different subunits labeled by LW124 in *N. benthamiana* (**Figure 4a**, lane 2, bands 3 and  
210 4). Co-labeling of MVB072 with LW124 shows two signals for LW124 and one signal for MVB072  
211 (**Figure 4a**, lane 4 overlay). The weak bottom MVB072 signal (band 2) is absent upon co-labeling  
212 with LW124, indicating that this signal is caused by  $\beta 1$ . Because the top MVB072 signal (band 1) also  
213 contains  $\beta 1$  (Misas-Villamil et al., 2013), both MVB072 signals contain  $\beta 1$ , consistent with the two  
214 signals displayed by LW124. The overlay, however, shows that the two MVB072 signals migrate  
215 slower in the gel than the two LW124 conjugates (**Figure 4a**, lanes 1 and 2), which is consistent with  
216 the MW shift seen for Arabidopsis, and is explained from the fact that MVB072 is larger and more  
217 bulkier when compared to LW124 (**Figures 1a** and **2a**).

218 MVB127 labeling shows one specific signal at 28 kDa (**Figure 4a**, lane 3, band 5). Co-  
219 labeling of MVB072 with MVB127 causes a more intense bottom signal, caused by an overlap of the  
220  $\beta 1$ -MVB072 and  $\beta 5$ -MVB127 conjugates. The observation that the  $\beta 5$ -MVB127 conjugate migrates  
221 faster through the protein gel than the  $\beta 5$ -MVB127 conjugate is consistent with the MW shift seen for

222 Arabidopsis, and is explained from the fact that MVB072 is larger and more bulkier when compared  
223 to MVB127 (**Figures 1a** and **2a**). LW124 and MVB127 co-labeling results in two signals for LW124  
224 and one signal for MVB127 (**Figure 4a**, lane 6).

225 Pre-incubation with N3 $\beta$ 1 and N3 $\beta$ 5 confirms that the lowest MVB072 signal (**Figure 4b**,  
226 band 2) and the two LW124 correspond to  $\beta$ 1 (**Figure 4b**, bands 3 and 4), whereas the MVB127 signal  
227 corresponds to  $\beta$ 5 (**Figure 4b**, band 5), supporting the specificity of  $\beta$ 1 and  $\beta$ 5 labeling by LW124 and  
228 MVB127, respectively (**Figure 4b**, lanes 5-12). There is, however, some reciprocal suppression of  
229 N3 $\beta$ 1 on MVB127( $\beta$ 5) and N3 $\beta$ 5 on LW124( $\beta$ 5) (**Figure 4b**, lanes 5, 6, 9 and 11).

230

231 *Phylogenetic and proteomic analysis reveals multiple incorporated proteasome subunits in N.*  
232 *benthamiana*

233 The detection of two  $\beta$ 1 signals in *N. benthamiana* using LW124 is remarkable, since the Arabidopsis  
234 genome has only one gene encoding  $\beta$ 1, and  *$\beta$ 1din* in tobacco is defence induced (Suty et al., 2003).  
235 We therefore searched the *N. benthamiana* genome (<https://solgenomics.net/>) for genes encoding  
236 catalytic subunits of the proteasome. Blast searches for catalytic subunits resulted in six predicted  $\beta$ 1  
237 proteins, three  $\beta$ 2 proteins and three  $\beta$ 5 proteins. Phylogenetic analysis revealed that the paralogous  
238 subunits are more related to each other than to the subunits of Arabidopsis, except for  $\beta$ 1, where two  
239 groups seem to exist in *N. benthamiana* (**Figure 5**). One  $\beta$ 1 and one  $\beta$ 2 subunit are shorter than their  
240 respective paralogs. We consider these pseudogenes since their predicted MW is too low to explain the  
241 signals we detect upon labeling.

242 To determine if these genes also encode for proteins that are part of the active proteasome in  
243 leaves, we performed mass spectrometry analysis of two different pull down experiments of *N.*  
244 *benthamiana* leaf extracts labeled with MVB072. To also detect an altered subunit assembly during  
245 defence, the pull down was performed on plants treated with the SA analog benzothiadiazole (BTH),  
246 whereas the other pull down was performed on the mock control. Each pull down assay was analyzed  
247 twice by MS and 45 peptides were detected of the catalytic subunits, of which 11 were unique  
248 (Supplemental **Table S1** and **Figure S3**).

249 In these experiments we identified unique peptides of two different  $\beta$ 1 subunits:  $\beta$ 1a and  $\beta$ 1b  
250 (**Figures 5b**, **5c** and **S2**). Several peptides that are shared with one other protein (dark grey) map to the  
251 truncated  $\beta$ 1 subunit (NbS00011733g0005.1) (dark grey in **Figure 5c**). The truncated subunit would  
252 migrate at a predicted 16.7 kDa, but we do not detect fluorescent signals in this region. Removal of  
253 this subunit from the analysis would add two additional unique peptides to one of the already  
254 identified  $\beta$ 1a subunit (NbS0009991g0103.1). The presence of two  $\beta$ 1 subunits having a different  
255 predicted MW of 23.7 ( $\beta$ 1a) and 22.6 ( $\beta$ 1b) kDa is consistent with the two LW124 signals detected  
256 upon labeling.

257 We also detected unique peptides for two  $\beta$ 2 subunits ( $\beta$ 2a and  $\beta$ 2b) and one  $\beta$ 5 subunit ( $\beta$ 5a)  
258 (**Figure 5b**). Two other  $\beta$ 5 subunit peptides do not match to this identified  $\beta$ 5a protein, indicating that

259 there must be a second  $\beta 5$  subunit ( $\beta 5b$ ), which is either Nb00003340g0007.1 or the shorter  
260 NbS00002498g0003.1 (**Figures 5b** and **5c**). These findings confirm an expanded repertoire of  
261 catalytic proteasome subunits in active proteasomes of *N. benthamiana*.

262 Comparison of the identified proteasome subunits from water- and BTH-treated plants did not  
263 reveal significant differences (**Figure 5b**). These data suggest that the active catalytic proteasome  
264 subunit incorporation is not different during SA-induced defence. However, more quantitative  
265 proteomic analysis with more samples may be required to rule out any changes upon BTH treatment.

266

267 *Bacterial infections affect active subunit composition in N. benthamiana.*

268 We next used the subunit-selective probes to investigate changes in the proteasome subunit  
269 composition during biotic stress. We therefore infected *N. benthamiana* leaves with *P. syringae* pv.  
270 *tomato* DC3000 (PtoDC3000), which triggers a non-host response (NHR, or effector-triggered  
271 immunity (ETI)) because it produces type-III effector hopQ1-1, which is recognized in *N.*  
272 *benthamiana*. We also included the  $\Delta$ hopQ1-1 mutant of PtoDC3000 (PtoDC3000( $\Delta$ hQ)), which  
273 causes disease on *N. benthamiana* (Wei et al., 2007).

274 Unexpectedly, whilst the proteasome labeling upon infection with PtoDC3000( $\Delta$ hQ) is highly  
275 reproducible, we noticed that proteasome labeling upon infection with PtoDC3000(WT) differs  
276 significantly between eight independent infection assays. MVB072 labeling of extracts of  
277 PtoDC3000(WT)-infected leaves indicates that the activity of the proteasome is either upregulated  
278 (**Figure 6a**), or down regulated (**Figure 6b**). Importantly, labeling the same extracts with  
279 LW124+MVB127, provides much more insight. The lower  $\beta 1$  signal either intensifies strongly upon  
280 PtoDC3000(WT) infection (**Figure 6c**, Supplemental **Figures S4-S5**), or only slightly (**Figure 6d**,  
281 Supplemental **Figures S6-S8**). Remarkably, however, the  $\beta 5$  signal is either induced (**Figure 6c**,  
282 Supplemental **Figures S4-S5**) or strongly suppressed (**Figure 6d**, Supplemental **Figures S6-S8**). The  
283 fact that the ratio between  $\beta 1$  and  $\beta 5$  can differ between infection experiments significantly  
284 demonstrates that the activities of these two subunits can be uncoupled during bacterial infection. The  
285 cause of this phenotypic variation upon PtoDC3000(WT) infection is beyond the focus of the current  
286 manuscript, and is subject to further studies.

287 Proteasome activities upon infection by PtoDC3000( $\Delta$ hQ) show a robust 3-fold upregulation  
288 in the intensity of the  $\beta 1$  and  $\beta 5$  signals (**Figure 6e**, Supplemental **Figure S9**). Quantitative RT-PCR  
289 with gene-specific primers showed that also transcript levels of  $\beta 1a$ ,  $\beta 1b$  and  $\beta 5$  are significantly  
290 upregulated (**Figure 6f**), indicating that the differential proteasome activity upon PtoDC3000( $\Delta$ hQ) is  
291 mostly transcriptional. Notably, we detect a highly reproducible shift in the ratio between the two  $\beta 1$   
292 signals upon infection with PtoDC3000( $\Delta$ hQ) (**Figure 6g**).

293

294 **DISCUSSION**



295 We have introduced next generation subunit-specific probes for labeling the  $\beta 1$  and  $\beta 5$  proteasome  
296 catalytic subunits, and validated labeling in both *Arabidopsis thaliana* and *Nicotiana benthamiana*.  
297 We also introduced and validated subunit-selective inhibitors for the  $\beta 1$  and  $\beta 5$  subunits, which may  
298 be useful for chemical knockout assays. We discovered that the active *N. benthamiana* proteasome  
299 contains different paralogous catalytic subunits: two for  $\beta 1$ , two for  $\beta 2$  and two for  $\beta 5$ . Application of  
300 selective subunit labeling revealed and uncoupled induction in  $\beta 1$  and  $\beta 5$  subunits upon infection with  
301 virulent and avirulent *Pseudomonas syringae*.

302 Our data demonstrate that LW124 targets  $\beta 1$  and MVB127 targets  $\beta 5$ . Because the proteasome  
303 subunits of *Arabidopsis* have a distinct MW, we would have detected additional signals if LW124 and  
304 MVB127 would label additional catalytic subunits. Likewise, MVB127 should have caused an  
305 additional signal if it could label  $\beta 1$  of *N. benthamiana*. The absence of additional signals in  
306 *Arabidopsis* testifies the high selectivity of the subunit-selective probes.

307 By contrast, however, despite their structural similarity with the probes, the subunit-selective  
308 inhibitors partially suppress reciprocal labeling: N3 $\beta 1$  suppresses labeling of  $\beta 5$  by MVB127 and  
309 N3 $\beta 5$  suppresses labeling by LW124, in both *Arabidopsis* (**Figure 2b**) and *N. benthamiana* (**Figure**  
310 **4b**). Likewise, we detect a consistent suppression of  $\beta 5$  labeling by MVB127 upon colabeling with  
311 LW124 (**Figures 1c, 2b, 4a and 4b**). Although we can not exclude at this stage that N3 $\beta 1$  and N3 $\beta 5$   
312 are weak inhibitors of  $\beta 5$  and  $\beta 1$ , respectively, the fact that the corresponding probes are subunit  
313 selective suggest an alternative explanation. The suppression of labeling by inhibitors and probes that  
314 target other subunits may also be caused by crowding of the proteolytic chamber (inhibitor bound to  
315 one subunit hinders access of probes to another subunit) or allosteric regulation (inhibition of one  
316 subunits affects labeling efficiency of another subunit). Although the proteolytic chamber is probably  
317 too large to support the crowded chamber hypothesis, the catalytic subunits of the proteasome are  
318 known to allosterically regulate each other, e.g. to facilitate the cyclical bite-chew mechanism  
319 (Kisselev et al., 1999).

320

321 *N. benthamiana* assembles different proteasomes

322 LW124 labeling of *N. benthamiana* displays two different  $\beta 1$  signals. MS analysis of MVB072 labeled  
323 proteins confirmed that at least two different  $\beta 1$  proteins are incorporated in proteasomes as active  
324 catalytic subunits. Subunits that are not incorporated into the proteasome remain in the inactive  
325 precursor state and are probably degraded (Chen & Hochstrasser, 1996). MS analysis of MVB072-  
326 labeled proteins also revealed at least two different  $\beta 2$  proteins and two different  $\beta 5$  subunits that must  
327 have been part of an active proteasome. However, MVB127 labeling only displays one  $\beta 5$  signal,  
328 indicating that the labeled proteins run at the same height. The fact that multiple paralogs were  
329 identified demonstrates that *N. benthamiana* produces diverse catalytic subunits and might assemble  
330 different proteasomes.

331 The concept that plants can assemble multiple proteasomes is supported by the finding that  
332 Arabidopsis also incorporates paralogous subunits into the 26S proteasome (Yang et al., 2004; Book et  
333 al., 2010). Remarkably, little is known about the role of paralogous CP subunits but more about  
334 paralogous RP subunits. Different paralogs of a subunit may act redundantly. For example, the RPN1  
335 subunit in Arabidopsis is encoded by two genes, *RPN1a* and *RPN1b*, which differ in their expression  
336 pattern (Yang et al., 2004). Nevertheless, *rpn1a* mutant lines maintain a functional proteasome  
337 indicating a redundant function (Wang et al., 2009). RPT2 and RPT5 isoforms also share redundant  
338 functions (Lee et al., 2011). In both Arabidopsis and maize, RPT2 and RPT5 are encoded by the  
339 paralogous genes *RPT2a - RPT2b* and *RPT5a - RPT5b*, respectively (Book et al., 2010). However,  
340 there are cases where paralogous subunits seem to have different functions. For example, *RPT5b*  
341 complements *RPT5a* in the *Col* ecotype, but not in *Ws* ecotype (Gallois et al., 2009), demonstrating an  
342 ecotype-dependent redundancy but also indicating alternative functions for the different isoforms. *N.*  
343 *benthamiana* is an allotetraploid, and the ancient genome duplication may explain a duplication of the  
344 proteasome subunits genes. At this stage, it is unclear if the different paralogous proteins have  
345 different functions.

346

#### 347 *Modification of the proteasome upon bacterial infection.*

348 Interestingly, subunit-selective proteasome activity profiling revealed that the activity of the catalytic  
349  $\beta 5$  subunit can be strongly induced or suppressed upon infection with *Pseudomonas syringae* and  
350 show that the activities of  $\beta 1$  and  $\beta 5$  can be uncoupled during infection. Uncoupling is not expected  
351 for proteasome complexes that incorporate equal numbers of catalytic subunits, but may have been  
352 caused by selective subunit inhibition during infection with *P. syringae*, or the specific activation of  
353 the  $\beta 1$  subunit during NHR/ETI responses.

354 Mammals have inducible subunits that can replace other  $\beta$  subunits, e.g. to create the  
355 immunoproteasome (Aki et al., 1994). Immunoproteasomes exhibit modified peptidase activities and  
356 variable cleavage site preferences. Their main function is the maintenance of cell homeostasis and cell  
357 viability under oxidative conditions (Seifert et al., 2010). It is likely that plants also possess a type of  
358 inducible proteasome where some catalytic subunits are replaced under biotic or abiotic stresses. We  
359 have identified six genes encoding  $\beta 1$  catalytic subunits from the *N. benthamiana* genome, suggesting  
360 that the other isoforms that we did not detect by MS analysis are either expressed under different  
361 conditions, are tissue specific or are pseudogenes. This can also be the case for non identified  $\beta 2$  and  
362  $\beta 5$  proteins. Induction of genes encoding  $\alpha$  and  $\beta$  proteasome subunits has been described for tobacco  
363 cells treated with cryptogein (Dahan et al., 2001), whereas our earlier study revealed a post-  
364 translational upregulation of proteasome labeling upon treatment of Arabidopsis with benzodiazole  
365 (Gu et al., 2010). Transcript activation of proteasome genes after cryptogein treatment could be  
366 associated with oxidative stress, since attenuation of the oxidative burst blocks the expression of  
367  *$\beta 1din$* ,  *$\alpha 3din$*  and  *$\alpha 6din$*  genes (Suty et al., 2003).

368           Thus, different paralogous proteasome subunits might be assembled in active proteasomes  
369 under different conditions, for instance responding to oxidative stress. The encoded catalytic subunits  
370 in *N. benthamiana* carry only few polymorphic amino acid residues, and it is unknown at this stage to  
371 what extent they affect proteasome function, e.g. with respect to substrate selection and conversion.  
372 This study uncovers that more research is needed to investigate the occurrence and function of  
373 alternative proteasomes in plants.

374           Taken together, we have introduced subunit-specific probes to monitor the  $\beta 1$  and  $\beta 5$  subunits  
375 of the plant proteasome. The use of site-specific probes combined with phylogenetic and proteomic  
376 analysis revealed multiple isoforms for the  $\beta$  subunits, indicating that different proteasomes co-exist in  
377 leaves. The subunit selective probes revealed unexpected, uncoupled differential activities of  $\beta 1$  and  
378  $\beta 5$  upon bacterial infection, that raise exciting questions on the underlying mechanism and biological  
379 role in immunity.

380

381

## 382 **EXPERIMENTAL PROCEDURES**

### 383 *Probes and inhibitors*

384 The synthesis of LW124, MVB127, N3 $\beta 1$  and N3 $\beta 5$  has been described previously (Verdoes et al.,  
385 2010; Li et al., 2013). As with our previously introduced probes, aliquots of these chemicals are  
386 available upon request and frequent use may accelerate their commercial availability.

387

### 388 *Plant material and labeling conditions*

389 *Arabidopsis thaliana* ecotype Col-0 and *Nicotiana benthamiana* plants were grown in the greenhouse  
390 under a regime of 14 h light at 20 °C. 3–5 weeks old plants were used for labeling experiments. For *in*  
391 *vitro* labeling, leaves were ground in water containing 10 mM DTT and extracts were cleared by  
392 centrifugation. Labeling was performed by incubating the protein extract in 60  $\mu$ l buffer containing  
393 66.7 mM Tris pH 7.5 and 0.5 – 0.8  $\mu$ M probe for 2 h at room temperature (22–25 °C) in the dark.  
394 After acetone precipitation pellets were re-suspended in 40  $\mu$ l 1x loading buffer and samples were  
395 separated on 12% SDS gel. Inhibitory assays were performed by 30 min pre-incubation of protein  
396 extracts with 50  $\mu$ M of the inhibitor of interest, followed by 2 h labeling. For *in vivo* inhibition of the  
397 proteasome 50  $\mu$ M of the inhibitor was infiltrated in *N. benthamiana* leaves using a syringe without a  
398 needle. After 6 h incubation at room temperature, a leaf disc (1.6 cm diameter) of the infiltrated area  
399 was collected and labeled with the probe of interest as described above. Labeled proteins were  
400 visualized by in-gel fluorescence scanning using a Typhoon FLA 9000 scanner (GE Healthcare,  
401 <http://www.gelifesciences.com>) with Ex473/Em530 nm for LW124 and Ex532/Em580 nm for  
402 MVB127, MVB072 and RhSylA. Fluorescent signals were quantified using ImageQuant 5.2 (GE  
403 Healthcare) with the rolling ball method for background correction. To confirm equal loading,  
404 Coomassie brilliant blue or SyproRuby (Invitrogen) staining was performed according to the

405 instructions of the manufacturer. SyproRuby gels were fluorescent scanned (Ex472/Em580 nm) and  
406 used for loading correction in the quantification of fluorescent signals. Statistical significance was  
407 calculated with a student's t-test of at least three replicates.

408

#### 409 *Large scale pull down assay*

410 Large scale pull down experiments were performed once on plants treated with benzothiadiazole  
411 (BTH) and once on the water control. This material was generated by spraying 3-4-week old *N.*  
412 *benthamiana* plants with 0.13 mg/mL BTH (BION, Syngenta) containing 0.01% Silwet L-77 (Lehle  
413 Seeds) or sprayed with water containing the same concentration of Silwet L-77. Leaves were  
414 harvested two days after treatment. 44 leaf discs of 2.3 cm diameter were collected per sample and  
415 ground in a buffer containing 1 mM DTT and 67 mM Tris pH 7.5. After centrifugation, 10 ml of  
416 protein extract was used for labeling with 20  $\mu$ M MVB072 or 2.5  $\mu$ l DMSO. Samples were incubated  
417 at room temperature and in the dark with gentle shaking for 2 h. Labeling was stopped by precipitating  
418 total proteins via the chloroform/methanol precipitation method (Wessel and Flügge, 1984). Affinity  
419 purification and in-gel digestion was performed as described elsewhere (Chandrasekar et al., 2014).

420

#### 421 *Mass spectrometry*

422 LC-MS/MS Experiments were performed on an Orbitrap Elite instrument (Thermo, Michalski et al.  
423 2012) that was coupled to an EASY-nLC 1000 liquid chromatography (LC) system (Thermo). The LC  
424 was operated in the one-column mode. The analytical column was a fused silica capillary (75  $\mu$ m  $\times$  15  
425 cm) with an integrated PicoFrit emitter (New Objective) packed in-house with Reprosil-Pur 120 C18-  
426 AQ 1.9  $\mu$ m resin (Dr. Maisch). The LC was equipped with two mobile phases: solvent A (0.1% formic  
427 acid, FA, in water) and solvent B (0.1% FA in acetonitrile, ACN). All solvents were of UPLC grade  
428 (Sigma). Peptides were directly loaded onto the analytical column with a maximum flow rate that  
429 would not exceed the set pressure limit of 800 bar (usually around 0.7 – 0.8  $\mu$ l/min). Peptides were  
430 subsequently separated on the analytical column by running a 60 min or 120 min gradient of solvent A  
431 and solvent B (60 min runs: start with 2% B; gradient 2% to 10% B for 2.5 min; gradient 10% to 35%  
432 B for 45 min; gradient 35% to 45% B for 7.5 min; gradient 45% to 100% B for 2 min and 100% B for  
433 3 min. 120 min runs: start with 2% B; gradient 2% to 10% B for 5 min; gradient 10% to 35% B for 90  
434 min; gradient 35% to 45% B for 15 min; gradient 45% to 100% B for 4 min and 100% B for 6 min.) at  
435 a flow rate of 300 nl/min. The mass spectrometer was operated using Xcalibur software (version 2.2  
436 SP1.48). The mass spectrometer was set in the positive ion mode. Precursor ion scanning was  
437 performed in the Orbitrap analyzer (FTMS) in the scan range of  $m/z$  300-1800 and at a resolution of  
438 60000 with the internal lock mass option turned on (lock mass was 445.120025  $m/z$ , polysiloxane)  
439 (Olsen et al., 2005). Product ion spectra were recorded in a data dependent fashion in the ion trap  
440 (ITMS) in a variable scan range and at a rapid scan rate. The ionization potential (spray voltage) was  
441 set to 1.8 kV. Peptides were analyzed using a repeating cycle consisting of a full precursor ion scan

442 (1.0 × 10<sup>6</sup> ions or 200 ms) followed by 15 product ion scans (1.0 × 10<sup>4</sup> ions or 50 ms) where peptides  
443 are isolated based on their intensity in the full survey scan (threshold of 500 counts) for tandem mass  
444 spectrum (MS2) generation that permits peptide sequencing and identification. CID collision energy  
445 was set to 35% for the generation of MS2 spectra. For the 2 h gradient length the data dependent  
446 decision tree option and supplemental activation was switched on. The ETD reaction time was 100 ms.  
447 During MS2 data acquisition dynamic ion exclusion was set to 30 seconds with a maximum list of  
448 excluded ions consisting of 500 members and a repeat count of one. Ion injection, time prediction,  
449 preview mode for the FTMS, monoisotopic precursor selection and charge state screening were  
450 enabled. Only charge states higher than 1 were considered for fragmentation.

451

#### 452 *Peptide and Protein Identification using MaxQuant*

453 RAW spectra were submitted to an Andromeda (Cox et al., 2011) search in MaxQuant (version  
454 1.5.3.30) using the default settings (Cox et al., 2008) Match-between-runs was activated (Cox et al.,  
455 2014) MS/MS spectra data were searched against the in-house generated *Nicotiana benthamiana*  
456 database (78729 entries). All searches included a contaminants database (as implemented in  
457 MaxQuant, 267 sequences). The contaminants database contains known MS contaminants and was  
458 included to estimate the level of contamination. Andromeda searches allowed oxidation of methionine  
459 residues (16 Da) and acetylation of protein N-terminus (42 Da) as dynamic modification and the static  
460 modification of cysteine (57 Da, alkylation with iodoacetamide). Enzyme specificity was set to  
461 “Trypsin/P”. The instrument type in Andromeda searches was set to Orbitrap and the precursor mass  
462 tolerance was set to ±20 ppm (first search) and ±4.5 ppm (main search). The MS/MS match tolerance  
463 was set to ±0.5 Da. The peptide spectrum match FDR and the protein FDR were set to 0.01 (based on  
464 target-decoy approach). Minimum peptide length was 7 amino acids. The minimum score for modified  
465 peptides was 40.

466

#### 467 *Extraction of proteasome specific peptides*

468 The peptide.txt output files from MaxQuant were loaded into Perseus v1.5.3.0. After removal of  
469 peptides matching to the reversed database and peptides matching to the contaminant database the  
470 remaining peptides were annotated using an in-house annotation file (annotation.wOG.txt). Peptides  
471 annotated to be derived from the proteasome or a proteasome subunit were extracted (Supplementary  
472 **Table S1**) and manually mapped to the individual proteasome sequences (Supplementary **Figure S2**).

473

#### 474 *Database search and phylogenetic analysis*

475 The *N. benthamiana* database (v. 0.4.4, 76,379 sequences) was downloaded from the SOL genomics  
476 network (<https://solgenomics.net>) and a blast search using Arabidopsis catalytic subunits as a template  
477 was performed. Additionally, *N. benthamiana* annotated T1 proteins found in the MEROPS database  
478 (<https://merops.sanger.ac.uk>) were compared with the hits obtained by the search with Arabidopsis

479 orthologs. The sequences were aligned with ClustalX2 (Larkin et al., 2007) standalone program. The  
480 alignment parameters were used as follows: the pair wise alignment gap opening penalty 30 and gap  
481 extension penalty 0.75, whereas for multiple alignment gap opening penalty were set to 15 and gap  
482 extension penalty to 0.3. Finally, the output alignment file from the ClustalX2 was used to generate  
483 the tree in R (Charif and Lobry, 2007; Paradis et al., 2004). The neighbor-joining algorithm was  
484 implemented in the script for the construction of the phylogenetic tree from the calculated distance  
485 matrix.

486

#### 487 *Bacterial infections*

488 For *P. syringae* infection, leaves of five-week old *N. benthamiana* plants were infiltrated using a  
489 needle-less syringe with  $10^6$  CFU/mL *Pseudomonas syringae* pv. *tomato* DC3000 and its *ΔhopQ1-1*  
490 mutant derivative (Wei et al., 2007). Three leaf discs (d=1 cm) were harvested at days 1 and 2. Leaf  
491 extracts were generated in 200 μL of 50 mM Tris buffer at pH 7.5 containing 5 mM DTT, cleared by  
492 centrifugation and labeled for two hours with 0.2 μM MVB072 or 0.8 μM LW124 + 0.8 μM MVB127  
493 at room temperature in the dark in 50 μL total volume.

494

#### 495 *Nucleic acid preparation, cDNA synthesis and qRT-PCR*

496 For RNA extraction, leaf material of *N. benthamiana* infected leaves was frozen in liquid nitrogen,  
497 ground to powder. The RNA was extracted using Trizol (Ambion), treated with DNase (QIAGEN),  
498 purified using the RNeasy Plant Mini Kit (QIAGEN) and used the SuperScript™ III Reverse  
499 Transcriptase (Invitrogen) for cDNA synthesis. The first-strand cDNA synthesis kit was used to  
500 reverse transcribe 1 μg of total RNA with oligo(dT) Primers. The qRT-PCR analysis was performed  
501 using the iQ SYBR Green Supermix (Bio-Rad) with an iCycler (Bio-Rad). Specific primers were used  
502 to amplify *β1a* (forward: 5'-ctgctggatattgtgcctgc-3', reverse: 5'-ggctcaaacatgctgcagct-3'), *β1b*  
503 (forward: 5'-tgcccctattcacgtgttg-3', reverse: 5'-gttcagcaggacaaaagga-3'), *β5b* (forward: 5'-  
504 ctcccattctacgtgctca-3', reverse: 5'-ggattgacttgcttagctcac-3') and *PP2A* (forward: 5'-  
505 gacctgatgttgatgttcgct-3', reverse: 5'-gagggattgaagagagatttc-3') was used as reference gene for  
506 normalization. Cycling conditions were as follows: 3 min at 95°C, followed by 45 cycles of 15 sec at  
507 95°C, 15 sec at 60°C and 30 sec at 72°C. After each PCR, the specificity of the amplified product was  
508 verified with the melting curves. Gene expression levels for *β1a*, *β1b* and *β5a* were then calculated  
509 relative to *PP2A* using the 2- $\Delta$ Ct (cycle threshold) method (Livak and Schmittgen, 2001). The average  
510 expression and the standard deviation of one experiment with four individuals were calculated, and  
511 expression of the mock control was set to 1. P values were calculated using a two tails *t*-test with  
512 unequal variance. P values <0.0005 were marked with three asterisks.

513

514

515 **ACKNOWLEDGEMENTS**

516 We would like to thank Prof. Gunther Doehleman and Prof. George Coupland for their support. We  
517 are grateful to Prof. Collmer for providing the  $\Delta$ hopQ1-1 mutant of PtoDC3000. This work was  
518 financially supported by the Max Planck Society, ERC Consolidator grant (R.H., grant No. 616449  
519 ‘GreenProteases’), an ERC starting grant (M.K., grant No. 258413), the Deutsche  
520 Forschungsgemeinschaft (M.K., grant no. INST 20876/127-1 FUGG) and the University of Oxford.

521 **REFERENCES**

- 522 **Aki, M., Shimbara, N., Takashina, M., Akiyama, K., Kagawa, S., Tamura, T., Tanahashi, N.,**  
523 **Yoshimura, T., Tanaka, K. and Ichihara, A.** (1994) Interferon-gamma induces different subunit  
524 organizations and functional diversity of proteasomes. *J. Biochem.* **115**, 257-269.
- 525 **Banfield, M.J.** (2015) Perturbation of host ubiquitin systems by plant pathogen/pest effector proteins.  
526 *Cell Microbiol.* **17**, 18-25.
- 527 **Book, A.J., Gladman, N.P., Lee, S.S., Scalf, M., Smith, L.M. and Vierstra, R.D.** (2010) Affinity  
528 purification of the Arabidopsis 26S proteasome reveals a diverse array of plant proteolytic complexes.  
529 *J. Biol. Chem.* **285**, 25554–25569.
- 530 **Carrión, C.A., Costa, M.L., Martínez, D.E., Mohr, C., Humbeck, K. and Guamet, J.J.** (2013) *In*  
531 *vivo* inhibition of cysteine proteases provides evidence for the involvement of 'senescence-associated  
532 vacuoles' in chloroplast protein degradation during dark-induced senescence of tobacco leaves. *J. Exp.*  
533 *Bot.* **64**, 4967-4980.
- 534 **Chandrasekar, B., Colby, T., Emon, A.E.K., Jiang, J., Hong, T.N., Villamor, J.G., Harzen, A.,**  
535 **Overkleeft, H.S. and Van der Hoorn, R.A.L.** (2014) Broad range glycosidase activity profiling. *Mol.*  
536 *Cell. Proteomics* **13**, 2787-2800.
- 537 **Charif, D. and Lobry, J.** (2007) SeqinR 1.0–2: a contributed package to the R project for statistical  
538 computing devoted to biological sequences retrieval and analysis. In: Structural Approaches to  
539 Sequence Evolution (Bastolla U., Porto M., Roman H. E., Vendruscolo M., eds), pp. 207–232,  
540 Springer, Berlin
- 541 **Chen, P. and Hochstrasser, M.** (1996) Autocatalytic subunit processing couples active site formation  
542 in the 20S proteasome to completion of assembly. *Cell* **86**, 961–972.
- 543 **Cox, J., Hein, M.Y., Lubner, C.A., Paron, I., Nagaraj, N. and Mann, M.** (2014) Accurate Proteome-  
544 wide Label-free Quantification by Delayed Normalization and Maximal Peptide Ratio Extraction,  
545 Termed MaxLFQ. *Mol. Cell. Proteomics* **13**, 2513-2526.
- 546 **Cox, J. and Mann, M.** (2008) MaxQuant enables high peptide identification rates, individualized  
547 p.p.b.-range mass accuracies and proteome-wide protein quantification. *Nat. Biotechnol* **26**, 1367-  
548 1372.
- 549 **Cox, J., Neuhauser, N., Michalski, A., Scheltema, R.A., Olsen, J.V. and Mann, M.** (2011)  
550 Andromeda: a peptide search engine integrated into the MaxQuant environment. *J. Proteome Res.* **10**,  
551 1794-1805.
- 552 **Cravatt, B.F., Wright, A.T. and Kozarich, J.W.** (2008) Activity-based protein profiling: from  
553 enzyme chemistry to proteomic chemistry. *Annu. Rev. Biochem.* **77**, 383–414.
- 554 **Dahan, J., Etienne, P., Petitot, A.S., Houot, V., Blein, J.P. and Suty, L.** (2001) Cryptogein affects  
555 expression of  $\alpha 3f$ ,  $\alpha 6$  and  $\beta 1$  proteasome subunits encoding gene in tobacco. *J. Exp. Bot.* **52**, 1947-  
556 1948.



557 **Dick, T.P., Nussbaum, A.K., Deeg, M., Heinemeyer, W., Groll, M., Schirle, M., Keilholz, W.,**  
558 **Stevanović, S., Wolf, D.H., Huber, R., Rammensee, H.G. and Schild, H.** (1998) Contribution of  
559 proteasomal  $\beta$ -subunits to the cleavage of peptide substrates analyzed with yeast mutants. *J. Biol.*  
560 *Chem.* **273**, 25637-25646.

561 **Dong, S., Stam, R., Cano, L.M., Song, J., Sklenar, J., Yoshida, K., Bozkurt, T.O., Oliva, R., Liu**  
562 **,Z., Tian, M., Win, J., Banfield, M.J., Jones, A.M., Van der Hoorn, R.A.L. and Kamoun, S.**  
563 (2014) Effector specialization in a lineage of the Irish potato famine pathogen. *Science* **343**, 552-555.

564 **Gallois, J.L., Guyon-Debast, A., Le´ cureuil, A., Vezon, D., Carpentier, V., Bonhomme, S. and**  
565 **Guerche, P.** (2009) The Arabidopsis proteasome RPT5 subunits are essential for gametophyte  
566 development and show accession-dependent redundancy. *Plant Cell* **21**, 442-459.

567 **Goodin, M.M., Zaitlin, D., Naidu, R.A. and Lommel, S.A.** (2008) *Nicotiana benthamiana*: Its  
568 history and future as a model for plant–pathogen interactions. *Mol. Plant-Microbe Interact.* **21**, 1015-  
569 1026.

570 **Greenbaum, D., Medzihradzky, K.F., Burlingame, A. and Bogyo, M.** (2000) Epoxide  
571 electrophiles as activity-dependent cysteine protease profiling and discovery tools. *Chem. Biol.* **7**, 569-  
572 581.

573 **Groll, M., Ditzel, L., Löwe, J., Stock, D., Bochtler, M., Bartunik, H.D. and Huber, R.** (1997)  
574 Structure of 20S proteasome from yeast at 2.4 Å resolution. *Nature* **386**, 463-471.

575 **Groll, M., Schellenberg, B., Bachmann, A.S., Archer, C.R., Huber, R., Powell, T.K., Lindow, S.,**  
576 **Kaiser, M. and Dudler, R.** (2008) A plant pathogen virulence factor inhibits the eukaryotic  
577 proteasome by a novel mechanism. *Nature* **452**, 755-758.

578 **Gu, C., Kolodziejek, I., Misas-Villamil, J.C., Shindo, T., Colby, T., Verdoes, M., Richau, K.H.,**  
579 **Schmidt, J., Overkleef, H.S. and Van der Hoorn, R.A.L.** (2010) Proteasome activity profiling: a  
580 simple, robust and versatile method revealing subunit-selective inhibitors and cytoplasmic, defence-  
581 induced proteasome activities. *Plant J.* **62**, 160-170.

582 **Gu, C.** (2009) Activity-based protein profiling in plants. PhD Thesis, University of Cologne.

583 **Hörger, A.C., Ilyas, M., Stephan, W., Tellier, A., Van der Hoorn, R.A.L. and Rose, L.E.** (2012)  
584 Balancing selection at the tomato RCR3 guardee gene family maintains variation in strength of  
585 pathogen defense. *PLoS Genetics* **8**, e1002813.

586 **Kaschani, F., Shabab, M., Bozkurt, T., Shindo, T., Schornack, S., Gu, C., Ilyas, M., Win, J.,**  
587 **Kamoun, S. and Van der Hoorn, R.A.L.** (2010) An effector-targeted protease contributes to defense  
588 against *Phytophthora infestans* and is under diversifying selection in natural hosts. *Plant Physiol.* **154**,  
589 1794-1804.

590 **Kisselev, A. F., Kopian, T. N., Castillo, V., and Goldberg, A. L.** (1999) Proteasome active sites  
591 allosterically regulate each other, suggesting a cyclical bite-chew mechanism for protein breakdown.  
592 *Mol. Cell* **4**, 395-402.

593 **Kolodziejek, I., Misas-Villamil, J.C., Kaschani, F., Clerc, J., Gu, C., Krahn, D., Niessen, S.,**  
594 **Verdoes, M., Willems, L.I., Overkleeft, H.S., Kaiser, M. and Van der Hoorn, R.A.L.** (2011)  
595 Proteasome activity imaging and profiling characterizes bacterial effector Syringolin A. *Plant Physiol.*  
596 **155**, 477-489.

597 **Kurepa, J. and Smalle, J.A.** (2008a) Structure, function and regulation of plant proteasomes.  
598 *Biochimie* **90**, 324-335.

599 **Larkin, M.A., Blackshields, G., Brown, N.P., Chenna, R., McGettigan, P.A., McWilliam, H.,**  
600 **Valentin, F., Wallace, I.M., Wilm, A., Lopez, R., Thompson, J.D., Gibson, T.J. and Higgins, D.G.**  
601 (2007) Clustal W and Clustal X version 2.0. *Bioinformatics* **23**, 2947-2948.

602 **Lee, K.H., Minami, A., Marshall, R.S., Book, A.J., Farmer, L.M., Walker, J.M. and Vierstra,**  
603 **R.D.** (2011) The RPT2 subunit of the 26S proteasome directs complex assembly, histone dynamics,  
604 and gametophyte and sporophyte development in Arabidopsis. *Plant Cell* **23**, 4298-4317.

605 **Li, N., Kuo, C.L., Paniagua, G., van den Elst, H., Verdoes, M., Willems, L.I., Van der Linden,**  
606 **W.A., Ruben, M., Van Genderen, E., Gubbens, J., Van Wezel, G.P., Overkleeft, H.S. and Florea,**  
607 **B.I.** (2013) Relative quantification of proteasome activity by activity-based protein profiling and LC-  
608 MS/MS. *Nat. Protocols* **8**, 1155-1168.

609 **Livak K.J. and Schmittgen, T.D.** (2001) Analysis of relative gene expression data using real-time  
610 quantitative PCR and the 2(-Delta Delta C(T)) Method. *Methods*. **25**, 402-408.

611 **Martínez, D.E., Bartoli, C.G., Grbic, V. and Guamet, J.J.** (2007) Vacuolar cysteine proteases of  
612 wheat (*Triticum aestivum* L.) are common to leaf senescence induced by different factors. *J. Exp. Bot.*  
613 **58**, 1099-1107.

614 **Michalski, A., Damoc, E., Lange, O., Denisov, E., Nolting, D., Muller, M., Viner, R., Schwartz,**  
615 **J., Belford, M., Dunyach, J.J., Cox, J., Horning, S., Mann, M. and Makarov, A.** (2012) Ultra high  
616 resolution linear ion trap Orbitrap mass spectrometer (Orbitrap Elite) facilitates top down LC MS/MS  
617 and versatile peptide fragmentation modes. *Mol. Cell. Proteomics* **11**, O111.013698.

618 **Misas-Villamil, J.C., Kolodziejek, I., Crabill, E., Kaschani, F., Niessen, S., Shindo, T., Kaiser,**  
619 **M., Alfano, J.R. and Van der Hoorn, R.A.L.** (2013) *Pseudomonas syringae* pv. *syringae* uses  
620 proteasome inhibitor Syringolin A to colonize from wound infection sites. *PLoS Pathogens* **9**,  
621 e1003281.

622 **Morimoto, K. and Van der Hoorn, R.A.L.** (2016) The increasing impact of activity-based protein  
623 profiling in plant science. *Plant Cell Physiol.* **57**, 446-461.

624 **Mueller, A.N., Ziemann, S., Treitschke, S., Aßmann, D. and Doehlemann, G.** (2013)  
625 Compatibility in the *Ustilago maydis*-maize interaction requires inhibition of host cysteine proteases  
626 by the fungal effector Pit2. *PLoS Pathog.* **9**, e1003177.

627 **Nguyen, H. M., Schippers, J. H., Goni-Ramos, O., Christoph, M. P., Dortay, H., Van der Hoorn,**  
628 **R. A. L., and Mueller-Roeber, B.** (2013) An upstream regulator of the 26S proteasome modulates  
629 organ size in *Arabidopsis thaliana*. *Plant J.* **74**, 25-36.

630 **Olsen, J.V., de Godoy, L.M., Li, G., Macek, B., Mortensen, P., Pesch, R., Makarov, A., Lange,**  
631 **O., Horning, S. and Mann, M.** (2005) Parts per million mass accuracy on an Orbitrap mass  
632 spectrometer via lock mass injection into a C-trap. *Mol. Cell. Proteomics* **4**, 2010-2021.

633 **Padmanabhan, A., Vuong, S.A. and Hochstrasser, M.** (2016) Assembly of an evolutionary  
634 conserved alternative proteasome isoform in human cells. *Cell Rep.* **14**, 2962-2974.

635 **Paradis, E., Claude, J. and Strimmer, K.** (2004) APE: analyses of phylogenetics and evolution in R  
636 language. *Bioinformatics* **20**, 289-290.

637 **Poret, M., Chandrasekar, B., Van der Hoorn, R.A.L. and Avice, J.B.** (2016) Characterization of  
638 senescence-associated protease activities in the efficient protein remobilization during leaf senescence  
639 of winter oilseed rape. *Plant Sci.* **246**, 139-153.

640 **Rooney, H., Van 't Klooster, J., Van der Hoorn, R.A.L., Joosten, M.H.A.J., Jones, J.D.G. and De**  
641 **Wit, P.J.G.M.** (2005) Cladosporium Avr2 inhibits tomato Rcr3 protease required for Cf-2-dependent  
642 disease resistance. *Science* **308**, 1783-1789.

643 **Schellenberg B., Ramel, C. and Dudler, R.** (2010) *Pseudomonas syringae* virulence factor  
644 Syringolin A counteracts stomatal immunity by proteasome inhibition. *Mol. Plant-Microbe Interact.*  
645 **23**, 1287-1293.

646 **Seifert, U., Bialy, L.P., Ebstein, F., Bech-Otschir, D., Voigt, A., Schröter, F., Prozorovski, T.,**  
647 **Lange, N., Steffen, J., Rieger, M., Kuckelkorn, U., Aktas, O., Kloetzel, P.M. and Krüger, E.**  
648 (2010) Immuno-proteasomes preserve protein homeostasis upon interferon-induced oxidative stress.  
649 *Cell* **142**, 613-624.

650 **Shabab, M., Shindo, T., Gu, C., Kaschani, F., Pansuriya, T., Chintha, R., Harzen, A., Colby, T.,**  
651 **Kamoun, S. and Van der Hoorn, R.A.L.** (2008) Fungal effector protein AVR2 targets diversifying  
652 defence-related Cys proteases of tomato. *Plant Cell* **20**, 1169-1183.

653 **Song, J., Win, J., Tian, M., Schornack, S., Kaschani, F., Muhammad, I., Van der Hoorn, RAL.**  
654 **and Kamoun, S.** (2009) Apoplastic effectors secreted by two unrelated eukaryotic plant pathogens  
655 target the tomato defense protease Rcr3. *Proc. Natl. Acad. Sci. USA* **106**, 1654-1659.

656 **Suty, L., Lequeu, J., Lancon, A., Etienne, P., Petitot, A.S. and Blein, J.P.** (2003) Preferential  
657 induction of 20S proteasome subunits during elicitation of plant defense reactions: towards the  
658 characterization of plant defense proteasomes. *Int. J. Biochem. Cell. Biol.* **35**, 637-650.

659 **Tian, M., Win, J., Song, J., Van der Hoorn, R.A.L., Van der Knaap, E. and Kamoun, S.** (2007) A  
660 *Phytophthora infestans* cystatin-like protein interacts with and inhibits a tomato papain-like apoplastic  
661 protease. *Plant Physiol.* **143**, 364-277.

662 **Üstün, S., Bartetzo, V. and Bornke, F.** (2013) The *Xanthomonas campestris* type III effector XopJ  
663 targets the host cell proteasome to suppress salicylic-acid mediated plant defence. *PLoS Pathog.* **9**,  
664 e1003427.

665 **Üstün, S., König, P., Guttman, D.S. and Börnke, F.** (2014) HopZ4 from *Pseudomonas syringae*, a  
666 member of the HopZ type III effector family from the YopJ superfamily, inhibits the proteasome in  
667 plants. *Mol. Plant-Microbe Interact.* **27**, 611-623.

668 **Üstün S, Sheikh A, Gimenez-Ibanez S, Jones A, Ntoukakis V, Börnke F.** (2016) The proteasome  
669 acts as a hub for plant immunity and is targeted by *Pseudomonas* type III effectors. *Plant Physiol.* **172**,  
670 1941-1958.

671 **Van der Hoorn, R.A.L., Leeuwenburgh, M.A., Bogyo, M., Joosten, M.H.A.J. and Peck, S.C.**  
672 (2004) Activity profiling of papain-like cysteine proteases in plants. *Plant Physiol.* **135**, 1170-1178.

673 **Van Esse, H.P., Van't Klooster, J.W., Bolton, M.D., Yadeta, K.A., Van Baarlen, P, Boeren, S.,**  
674 **Vervoort, J., De Wit, P.J.G.M. and Thomma, B.P.H.J.** (2008) The *Cladosporium fulvum* virulence  
675 protein Avr2 inhibits host proteases required for basal defense. *Plant Cell* **20**, 1948-1963.

676 **Verdoes, M., Willems, L.I., Van der Linden, W.A., Duivenvoorden, B.A., Van der Marel, G.A.,**  
677 **Florea, B.I., Kisselev, A.F. and Overkleeft, H.S.** (2010) A panel of subunit-selective activity-based  
678 proteasome probes. *Org. Biomol. Chem.* **8**, 2719-2727.

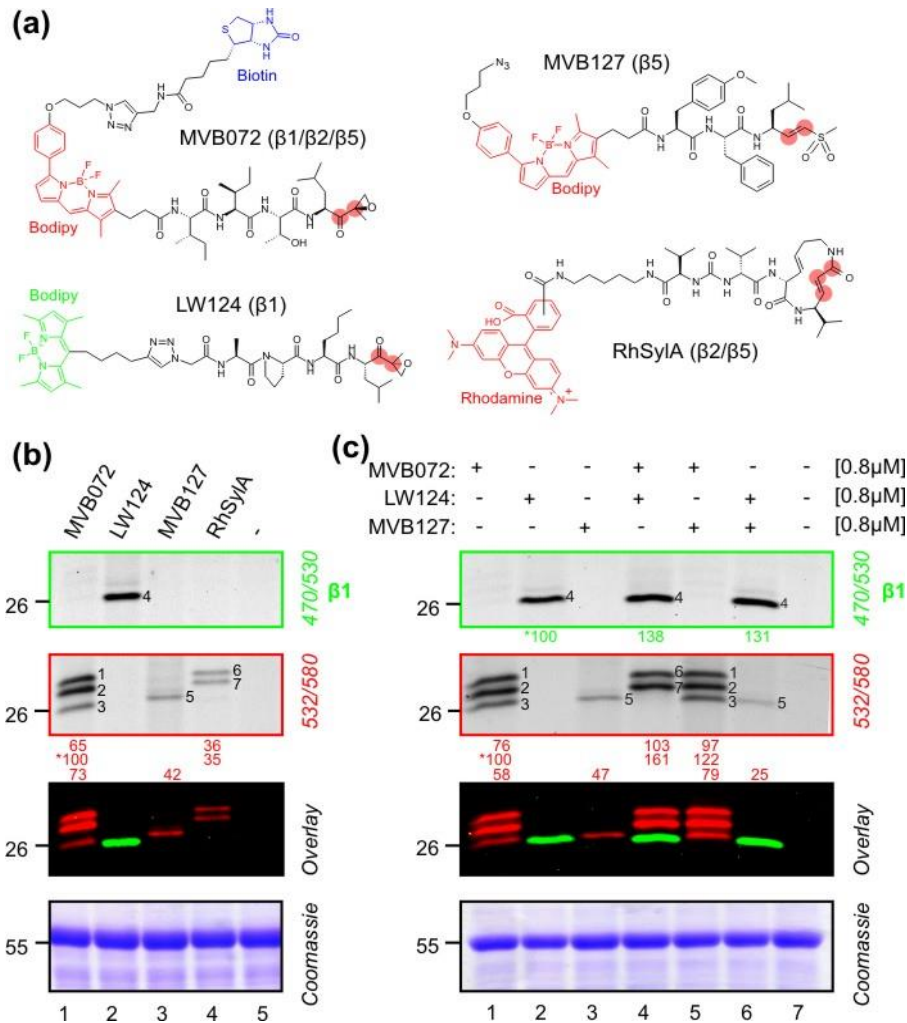
679 **Wang, S., Kurepa, J. and Smalle, J.A.** (2009) The Arabidopsis 26S proteasome subunit RPN1a is  
680 required for optimal plant growth and stress responses. *Plant Cell Physiol.* **50**, 1721-1725.

681 **Wei, C.F., Kvitko, B.H., Shimizu, R., Crabill, E., Alfano, J.R., Lin, N.C., Martin, G.B., Huang,**  
682 **H.C. and Collmer, A.** (2007) A *Pseudomonas syringae* pv. *tomato* DC3000 mutant lacking the type  
683 III effector HopQ1-1 is able to cause disease in the model plant *Nicotiana benthamiana*. *Plant J.* **51**,  
684 32-46.

685 **Wessel, D. and Flüggé, U.I.** (1984) A method for the quantitative recovery of protein in dilute-  
686 solution in the presence of detergents and lipids. *Anal. Biochem.* **138**, 141-143.

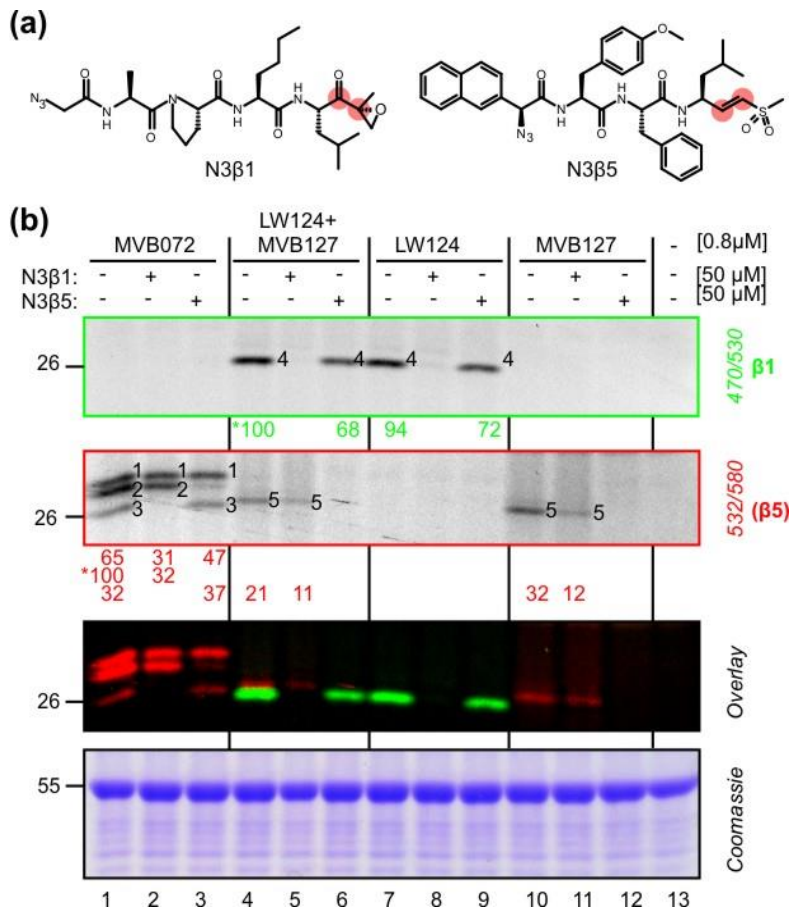
687 **Yang, P., Fu, H., Walker, J.M., Papa, C.M., Smalle, J.A., Ju, Y.M. and Vierstra, R.D.** (2004)  
688 Purification of the Arabidopsis 26S proteasome: biochemical and molecular analyses revealed the  
689 presence of multiple isoforms. *J. Biol. Chem.* **279**, 6401-6413.

690



691  
 692 **Figure 1.** Subunit-specific labeling of Arabidopsis proteasome catalytic subunits  
 693 (a) Structures of probes used in this study. MVB072 carries an epoxyketone reactive group, a Ile-Ile-  
 694 Ser-Leu tetrapeptide mimic and both a Bodipy TAMRA fluorophore (ex532/em580, red) and a biotin  
 695 affinity handle. LW124 contains an epoxyketone reactive group on a Ala-Pro-Nle-Leu tetrapeptide  
 696 mimic, and a Bodipy Cy2 fluorophore (ex470/em530, green). MVB127 carries a vinyl sulfone (VS)  
 697 reactive group, a MeTyr-Phe-Ile tripeptide and both an azide minitag and a Bodipy TAMRA  
 698 fluorophore (ex532/em580, red). RhSylA contains a Michael system reactive group embedded in a  
 699 syringolin A (SylA) structure and carries a Rhodamine fluorophore (ex532/em580, red). Sites that are  
 700 targeted by the catalytic Thr of the proteasome are highlighted with red circles.  
 701 (b) Comparison of the different labeling profiles generated with the four different probes. Arabidopsis  
 702 leaf extracts were labeled at pH 7.5 with 0.8  $\mu$ M MVB072, LW124 and MVB127 for 2 h and with 0.5  
 703  $\mu$ M RhSylA for 30 min. Fluorescent proteins were detected by in-gel fluorescent scanning at two  
 704 indicated settings. Numbers on the gel annotate signals caused by the labeled proteins. Numbers below  
 705 the gel show the intensity of the fluorescent signals, as a percentage compared to the reference signal  
 706 indicated by an asterisk. See **Figure S1** for entire gels. This experiment was performed at least three  
 707 independent times with similar results.

708 (c) (Co)labeling of proteasome subunits with the different probes. Arabidopsis leaf extracts were  
709 (co)labeled with MVB072, LW124, MVB127 for 2 h. Fluorescent proteins were detected as described  
710 in (b). This experiment has been reproduced at least three independent times with similar results.  
711



712

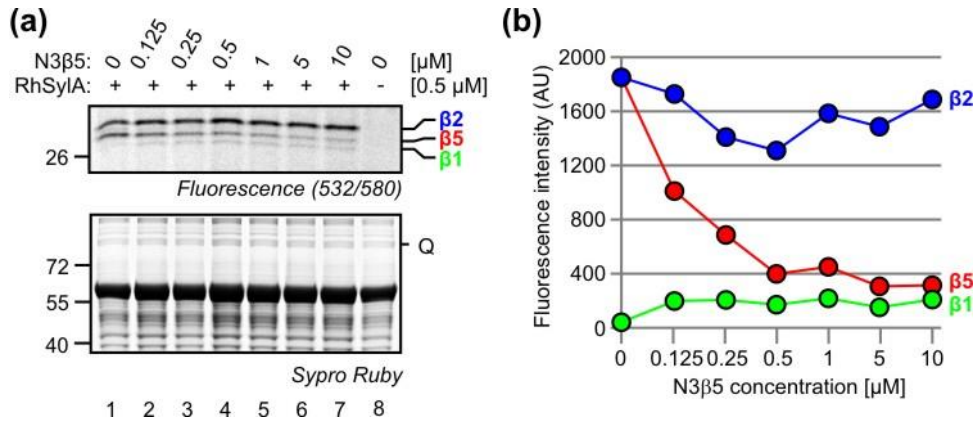
713 **Figure 2.** Subunit-selective inhibitors confirm selective subunit labeling

714 **(a)** Structures of specific inhibitors for the β1 and β5 proteasome catalytic subunits. N3β1 is an  
 715 epoxyketone specific inhibitor of the β1 catalytic subunit of the proteasome. N3β5 is a vinyl sulfone  
 716 based inhibitor that specifically targets the β5 catalytic subunit of the proteasome. Both inhibitors  
 717 contain an azide group. Reactive groups are indicated with red circles.

718 **(b)** Subunit-specific inhibitors confirm subunit-selective labeling by LW124 and MVB127.

719 Arabidopsis leaf extracts were pre-incubated with 50 μM N3β1 or N3β5 for 30 min, followed by  
 720 (co)labeling with MVB072, LW124 and MVB127 for 2 h. Fluorescent proteins were detected and

721 annotated with numbers as described in **Figure 1b**. The experiment has been reproduced at least three  
 722 independent times with similar results.



723

724

**Figure 3. Selective  $\beta 2$  labeling using [RhSylA + N3 $\beta 5$ ]**

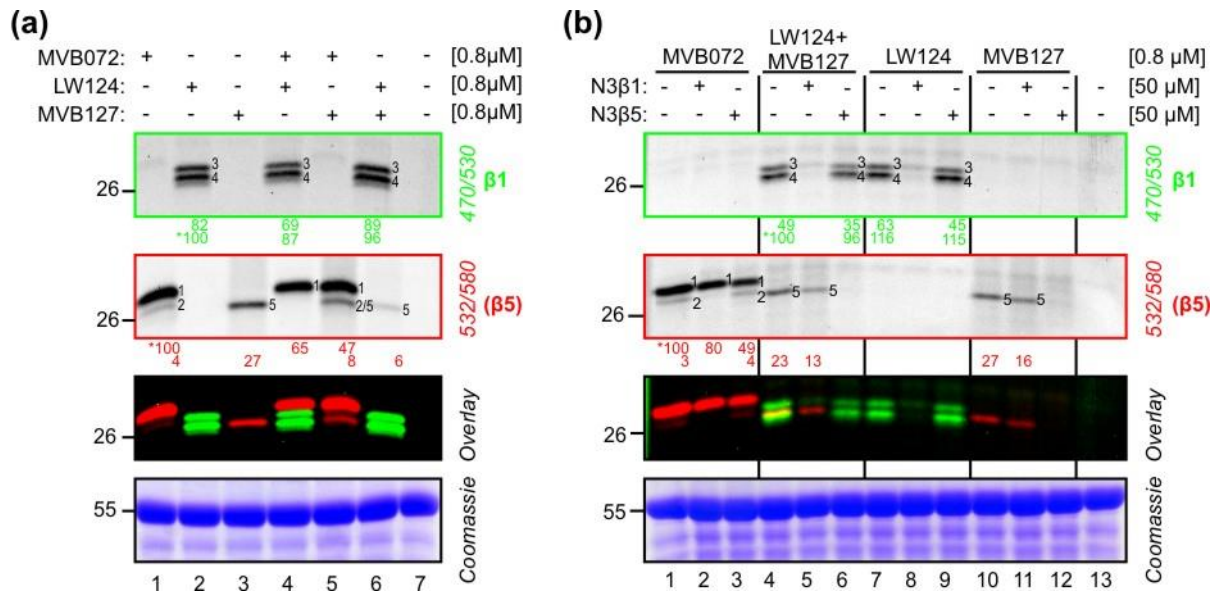
725

(a) In the presence of N3 $\beta 5$ , RhSylA labels  $\beta 2$  selectively. Arabidopsis leaf extracts were pre-  
 726 incubated with increasing concentrations of the  $\beta 5$  selective inhibitor N3 $\beta 5$  for 15 min followed by  
 727 labeling with  $0.5 \mu M$  RhSylA for 30 min. Proteins were detected by in-gel fluorescent scanning and  
 728 Sypro Ruby staining. This experiment has been repeated four independent times with similar results.

729

(b) Quantification of fluorescence labeling. Fluorescent signals corresponding to the catalytic subunits  
 730  $\beta 1$ ,  $\beta 2$  and  $\beta 5$  were quantified from fluorescent gels. Fluorescence intensity values were normalized  
 731 for loading using the Sypro Ruby signal Q, indicated in (a). Values for the catalytic subunits were  
 732 plotted against different N3 $\beta 5$  concentrations. A reproduction of this experiment is shown as Figure  
 733 S3.





734

735

**Figure 4.** Labeling of *N. benthamiana* proteasome with subunit-specific probes

736

**(a)** Labeling profiling of proteasome specific probes. *N. benthamiana* leaves extracts were (co)labeled at pH 7.5 with 0.8 μM MVB072, LW124 and MVB127 for 2 h. Fluorescent proteins were detected as described in **Figure 1b**. Numbers on gels annotate the different signals caused by labeled proteasome subunits. This experiment has been reproduced at least three independent times with similar results.

737

738

739

740

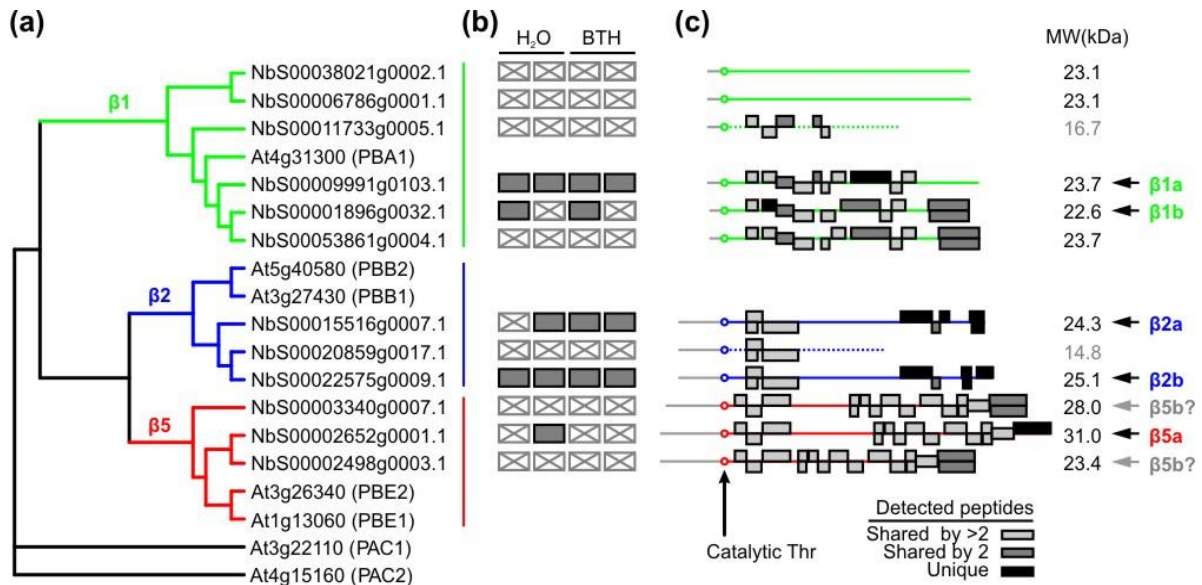
**(b)** Selective (co)labeling of β1 and β5 of *N. benthamiana*. *N. benthamiana* extracts were pre-incubated with 50 μM of the selective proteasome inhibitors N3β1 and N3β5 for 30 min followed by 2 h (co)labeling with 0.8 μM MVB072, LW124 and MVB127. Fluorescent proteins were detected as described in **Figure 1b**. Shown is a representative gel of three independent biological replicates.

741

742

743

744



745

746

**Figure 5.** Detection of the expanded proteasome subunit repertoire of *N. benthamiana*

747

(a) Neighbour-joining phylogenetic tree of  $\beta 1$ ,  $\beta 2$ , and  $\beta 5$  catalytic subunits of the proteasome of Arabidopsis and *N. benthamiana*, rooted with the  $\alpha 3$  subunit (PAC1 and PAC2).

749

(b) Identification of unique peptides upon MVB072 pull down from *N. benthamiana* leaf extracts.

750

Leaf extracts from plants treated with water or BTH were labeled with MVB072 and the labeled

751

proteins purified on avidin beads, eluted and separated on protein gels. Proteins were digested in-gel

752

with trypsin and the eluted peptides were analyzed twice by mass spectrometry. Filled grey boxes

753

indicate the detection of unique peptides of the respective proteasome subunit, whereas crossed boxes

754

indicate no unique peptides detected.

755

(c) Position of detected peptides of the catalytic subunits. Shown are the peptides that are unique

756

(black); shared with one other subunit (dark grey); or shared with more than one subunit (light grey).

757

Grey lines indicate the propeptide that is removed upon proteasome assembly. The mature protein

758

starts with a catalytic Thr residue. Truncated  $\beta 1$  and  $\beta 2$  proteasome subunits that may not be

759

functional are shown as dashed lines. The molecular weight (MW) indicates the calculated MW of the

760

mature subunit (without propeptide) in kilo Dalton (kDa). Black arrows indicate subunits that were

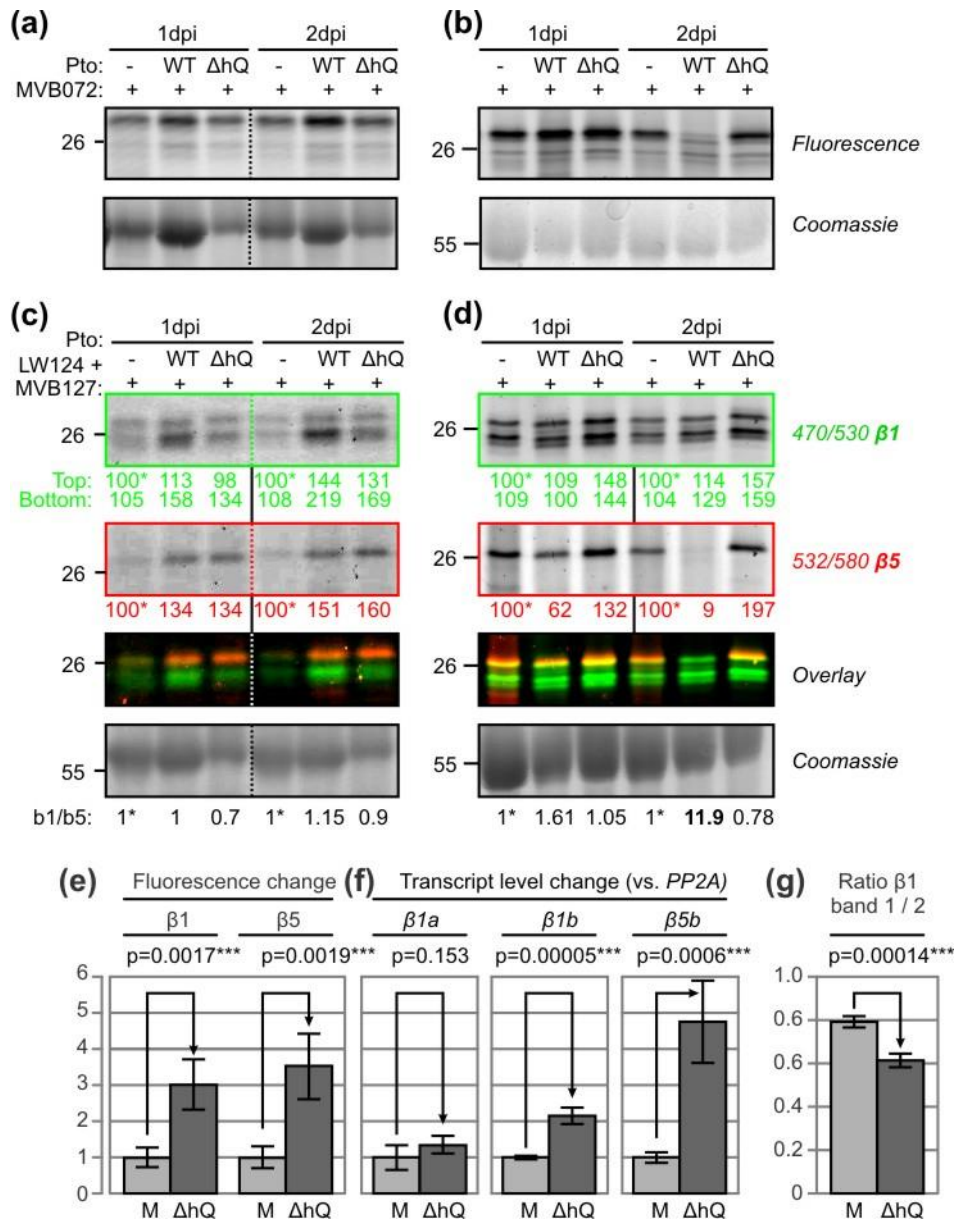
761

identified with unique peptide(s), and the grey arrow indicates the identified  $\beta 5$  subunit, in case the

762

truncated  $\beta 5$  subunit is considered non-functional.

763



764

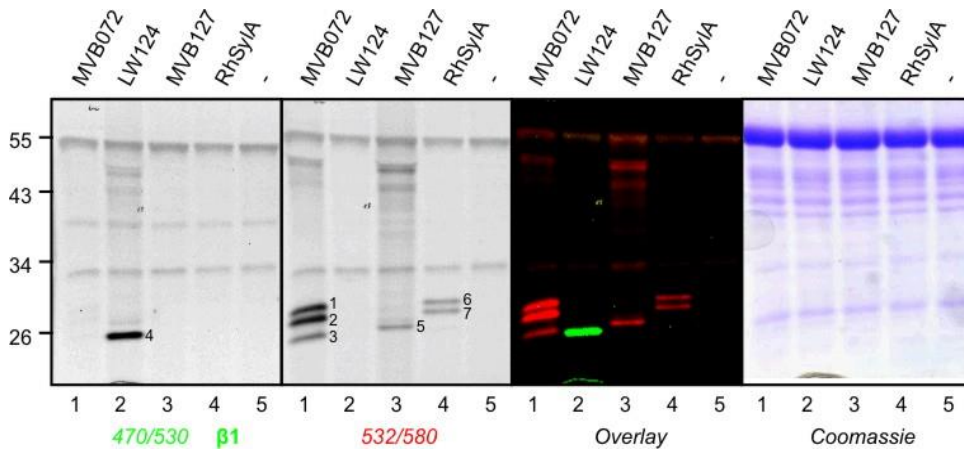
765 **Figure 6.** Uncoupled differential  $\beta 1$  and  $\beta 5$  activities upon bacterial infections.

766 **(a-g)** *N. benthamiana* leaves were infiltrated with buffer or  $10^6$  CFU/mL PtoDC3000(WT) or its  
 767 derived *ΔhopQ1-1* mutant PtoDC3000( $\Delta hQ$ ) and leaf disks were harvested at 1 and 2 dpi. Leaf  
 768 extracts were labeled with MVB072 **(a,b)** or LW124+MVB127 **(c,d)** and proteins were analyzed as  
 769 described in **Figure 1b**. Shown are representatives of independent experiments showing the two  
 770 different phenotypes, ranging from induced  $\beta 1/\beta 5$  activities (a,c; Supplemental **Figures S4-S5**), to  
 771 suppressed  $\beta 5$  activities (b,d; Supplemental **Figures S6-S8**). **(e)** Quantified fluorescence for  $\beta 1$   
 772 (LW124) and  $\beta 5$  (MVB127) in one experiment with four individuals (n=4 replicates). This experiment  
 773 was reproduced twice with similar results (Supplemental **Figures S9**). **(f)** Relative transcript levels of  
 774  $\beta 1a$ ,  $\beta 1b$  and  $\beta 5b$  relative to *PP2A* for the same experiment (n=4 individual plants) as shown in (e). **(g)**  
 775 Relative ratio of the two LW124 signals in the same experiment (n=4 replicates) as shown in (e). This  
 776 experiment was reproduced twice with similar results (Supplemental **Figure S9**).

777

778

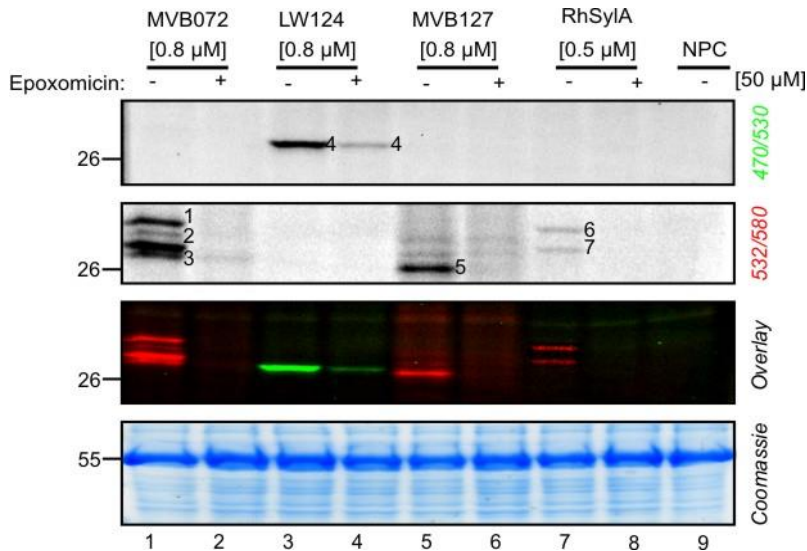
779 **SUPPLEMENTAL FIGURES**



780  
781 **Figure S1.** Entire gel showing selective labeling by different proteasome probes.

782 See legend of **Figure 1b** for more information

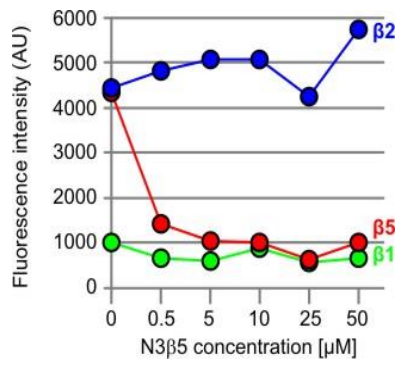
783



784  
785 **Figure S2.** Labeling is blocked by pre-incubation with epoxomicin.

786 Arabidopsis leaf extracts were pre-incubated with 50  $\mu$ M epoxomicin for 30 min and labeled with  
787 MVB072, LW124, MVB127 and RhSylA. Fluorescent proteins were detected at two indicated settings  
788 of the fluorescence scanner. Numbers on gels annotate different signals caused by labeled proteasome  
789 subunits.

790



791

792 **Figure S3.** Selective  $\beta 2$  labeling using [RhSylA + N3 $\beta 5$ ]

793 Arabidopsis leaf extracts were pre-incubated with increasing concentrations of the  $\beta 5$  selective  
 794 inhibitor N3 $\beta 5$  for 15 min followed by labeling with 0.5  $\mu\text{M}$  RhSylA for 30 min. Proteins were  
 795 detected by in-gel fluorescent scanning and Sypro Ruby staining. Fluorescent signals corresponding to  
 796 the catalytic subunits  $\beta 1$ ,  $\beta 2$  and  $\beta 5$  were quantified from fluorescent gels. Fluorescence intensity  
 797 values were normalized for loading using the Sypro Ruby signal. Values for the catalytic subunits  
 798 were plotted against different N3 $\beta 5$  concentrations.



799 **Beta 1**

800

801 >MER412180 - Nbs00038021g0002.1

802 MCIFISDSDESHQSN TTTIVGVTYDDGVILGSTDIIITQLTANVFLCHCALGAYTQVLLLEDARNFLDQETTAAVAEIVGMLLSAYDINNKNM

803 LRTGVLLGGWDKNGGGKIYEIGFSGVMEKSNFVGGYGTVDLNDFLEKEWKKMTEEEAEQLVVKALS LNNINS GCGVQTASVNSKEFTTAFH

804 PYATLP IKA EKLESEHMNEKPMLECI RAHLLLLLLNINEGL

805

806 >MER411609 - Nbs00006786g0001.1

807 MCIFIIDSEKSHQSN TTTIVGVTYDDGVMLGSTDIIITKLTA S VFLCHCALGADTQVLLLEDARNFLDQETTATVAEIVGMVLSAYDINNTKNM

808 LRTGVLLGGWDKNGGGKIYEIGFSGVMEKSNFVGGYGAVDLNDFLEKEWKKGLTEEEAEQLVVKALS LNNINS GCGAQTASVNSKGF TTFD

809 HPYVILP IKA EKLELENMNEKPMLECI RAHLLLLLLNIDEGL

810

811 >MER412281 - Nbs00011733g0005.1 coverage after T:

812 MDKSLLDVEQAHS MG TIIGVTYNRGVVLGANSRTSTGMYVANRASDKITQLTDNVYVCRSGSAADSQVVS DYVRYFLHQHMIQLGQPATVKVA

813 ANLVRLLSYNNKAMLQ TGMIVGGWDKYEGVKYMGFLLGAHSWNS LLLLEVCCQSVLFEYLILLPRSTLLVN

814

815 >MER412197 - Nbs00009991g0103.1 -  $\beta$ 1a coverage after T:

816 MDKSLLDVEQPHSMG TIIGVTYNGGVVLGADSRSTSTGMYVANRASDKITQLTDNVYVCRSGSAADSQVVS DYVRYFLHQHTIQLGQPATVKVA

817 ANLVRLLSYNNKAMLQ TGMIGGWDKYEGGKIYGVPLGGTLLLEQPF AIGGSGSSYLYGFFDQAWR EGMTQEAEAKLVVTA VSLAIARDGASGGV

818 VRTVTINKDGVTRKFPYGD TPLWHEEIEAVNSLLDIVPAASPEPMVS

819

820 >MER411801 - Nbs00001896g0032.1 -  $\beta$ 1b coverage after T:

821 MENTDQVDPHSMG TIIGVTYNGGVVLGADSRSTSTGMYVANRASDKITQLTDNVYVCRSGSAADSQIVSDYVRYFLHQHTIQLGQPATVKVAAN

822 LTRLQ TGMIGGWDKYEGGKIYGIPLGGTVLEQPF AIGGSGSSYLYGFFDQAWR EGMTQEAEAKLVVTA VSLAIARDGASGGVVRTVTINKDGA

823 TRKFPYGD SLQLWHEE LEPVNSLLDVVSASSPDPMVS

824

825 >MER411773 - Nbs00053861g0004.1 coverage after T:

826 MENTDQVDPHSMG TIIGVTYNGGVVLGADSRSTSTGMYVANRASDKITQLTDNVYVCRSGSAADSQIVSDYVRYFLHQHTIQLGQPATVKVAAN

827 LTRLQ TGMIGGWDKYEGGKIYGIPLGGTVLEQPF AIGGSGSSYLYGFFDQAWR EGMTQEAEAKLVVTA VSLAIARDGASGGVVRTVTINKDGA

828 TRKFPYGD SLQLWHEE LEPVNSLLDVVSASSPDPMVS

829

830 **Beta 2**

831

832 >MER411637 - Nbs00015516g0007.1 -  $\beta$ 2a coverage after T:

833 MASKAATDVPKGGGFSFDLCRRNEMLVNKLGRSPSFLKTG TIIVGLIFQDGVILGADTRATEGPIVADKNCEKIH YMAPNIYCCGAGTAADTEA

834 VTDMVSSQLKLRHRYHTGRESRVVTAL TLLKTHLFSYQGYVSAALVGGVDVTGPHLHTIYPHGSDTTLPYATMGSGSLAAMAIFESKYREGLSK

835 DEGIKLVAEAILSGVFNDLGS GSNVDICITR GNTEYLR NHMLPNPR TYPQKEVLLTKITPLRER VEVIEGGDAMEE

836

837 >MER411855 - Nbs00020859g0017.1

838 MTAKATMDVPQKGGGFSFDLCRRNEMLVNKLGRSPSFLKTG TIIVGLIFQDGVILGADTRATEGPIVADKNCEKIH YMAPNIYCCGAGTAADTEA

839 VTDMVSSQLKLRHRYHTGRESRVVTAL TLLKSHLFSYQGHVSAALVGGVDVTGPHLHTIYPHGSDTTLPYATNGLWFP RSNGLY

840

841 >MER411772 - Nbs00022575g0009.1 -  $\beta$ 2b coverage after T:

842 MTAKATMDVPQKGGGFSFDLCRRNEMLVNKLGRSPSFLKTG TIIVGLIFQDGVILGADTRATEGPIVADKNCEKIH YMAPNIYCCGAGTAADTEA

843 VTDMVSSQLKLRHRYHTGRESRVVTAL TLLKSHLFSYQGHVSAALVGGVDVTGPHLHTIYPHGSDTTLPYATMGSGSLAAMAIFESKYREGMNR

844 DEGIKLVAEAILSGVFNDLGS GSNVDICITR GNTEYLR NHLSPNRPTYPQKGYSPFK KTEVLLTR ITPLR EIVQVIEGGDAMEE

845

846

847 **Beta 5**

848

849 >MER412029 - Nbs00003340g0007.1 -  $\beta$ 5b coverage after T:

850 MMKIDFSGLEPTAPLKGESSVLCDGILSSPSFQIPNTNKEAIQMVKPAKG TTLAFIFKGGVMVAADSRASMGGYISSQSVKIIIEINPYMLG

851 TMAGGAADCQFWHRNLGIKKS GTQPKGMSDAKTS DLBGYP LNLGDALCESGKVESTAEPLKRLHELANKRRISVAGASKLLANILYSYRG

852 MGLSVGTMIAGWDEKGPGLYVVDSEGGRLKGNRFSVSGSPYAYGVLD SGYRFDLSVEEAAELARRAIYHATFRD GASGGVASVYHVGPNGWK

853 LSGDDV GELHYNYPVELESVEQEMA EVPVA

854

855 >MER411662 - Nbs00002652g0001.1 -  $\beta$ 5a coverage after T:

856 MMKIDFSGLEPTAPIKGESSELCDGILSSPSFQIPNATNFDGFQKEAIQMVKPAKG TTLAFIFKGGVMVAADSRASMGGYISSQSVKIIIEIN

857 PYMLGTMAGGAADCQFWHRNLGIKENANFVAIVILIDHHGLYKCKWPILKEDLIAVLEHLYKEGKEKKNMIVRGICAGWILLVVELCVVCRLH

858 ELANKRRISVAGASKLLANILYSYRGMGLSVGTMIAGWDEKGPGLYVVDSEGGRLKGNRFSVSGSPYAYGVLD SGYRFDLSVEEAAELARRAI

859 YHATFRD GASGGVASVYHVGPNGWK LSGDDV GELHYSYYPVELESVEQEMA EVPVA

860

861 >MER412196 - Nbs00002498g0003.1 coverage after T:

862 MMKIDFSGLEPTAPIKGESSELCDGILSSPSFQIPNATNFDGFQKEAIQMVKPAKG TTLAFIFKGGVMVAADSRASMGGYISSQSVKIIIEIN

863 PYMLGTMAGGAADCQFWHRNLGIKRLHELANKRRISVAGASKLLANILYSYRGMGLSVGTMIAGWDEKGPGLYVVDSEGGRLKGNRFSVSGS

864 PYAYGVLD SGYRFDLSVEEAAELARRAIYHATFRD GASGGVASVYHVGPNGWK LSGDDV GELHYNYPVELESVEQEMA EVPVA

865

866

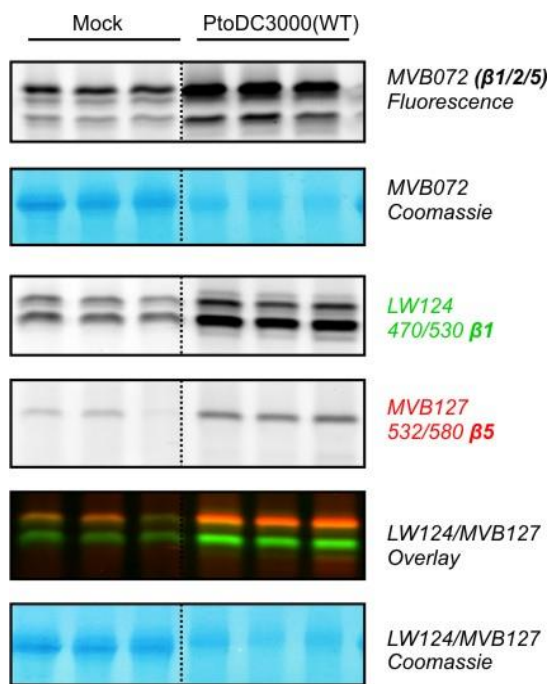
867 **Figure S3.** Identified peptides mapped on the protein sequences of the catalytic subunits of

868 the *N. benthamiana* proteasome. Shown are the catalytic Thr (blue); unique peptides (red);

869 peptides shared by two proteins (dark grey); peptides shared by more than two proteins (light grey);

870 peptides that overlap with a larger peptide (missed cleavage, underlined). Subunits that are too short

871 are printed with grey letters.

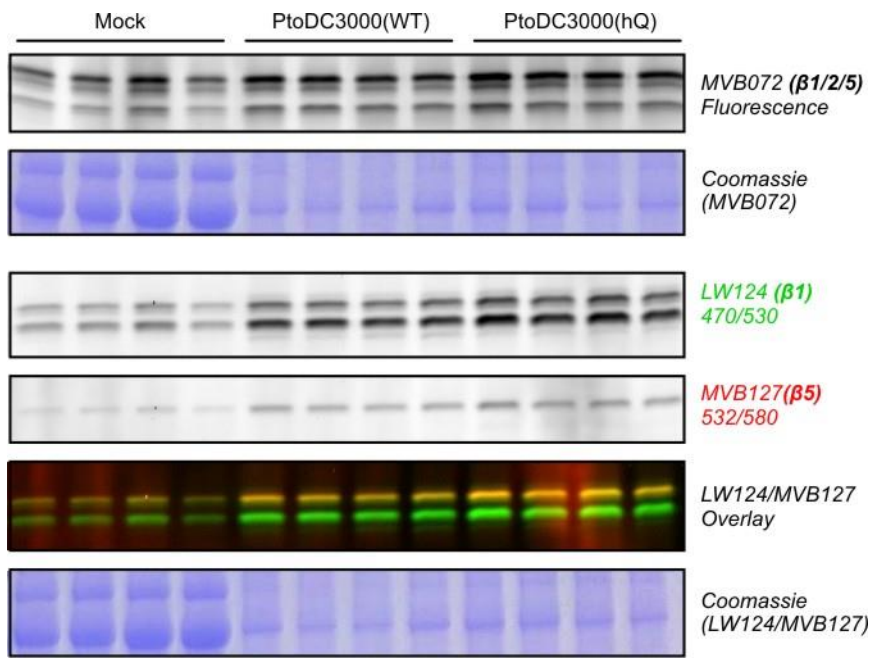


872

873 **Figure S4.** Increased proteasome activity upon WT infection. Shown is one experiment

874 containing three biological replicates.

875



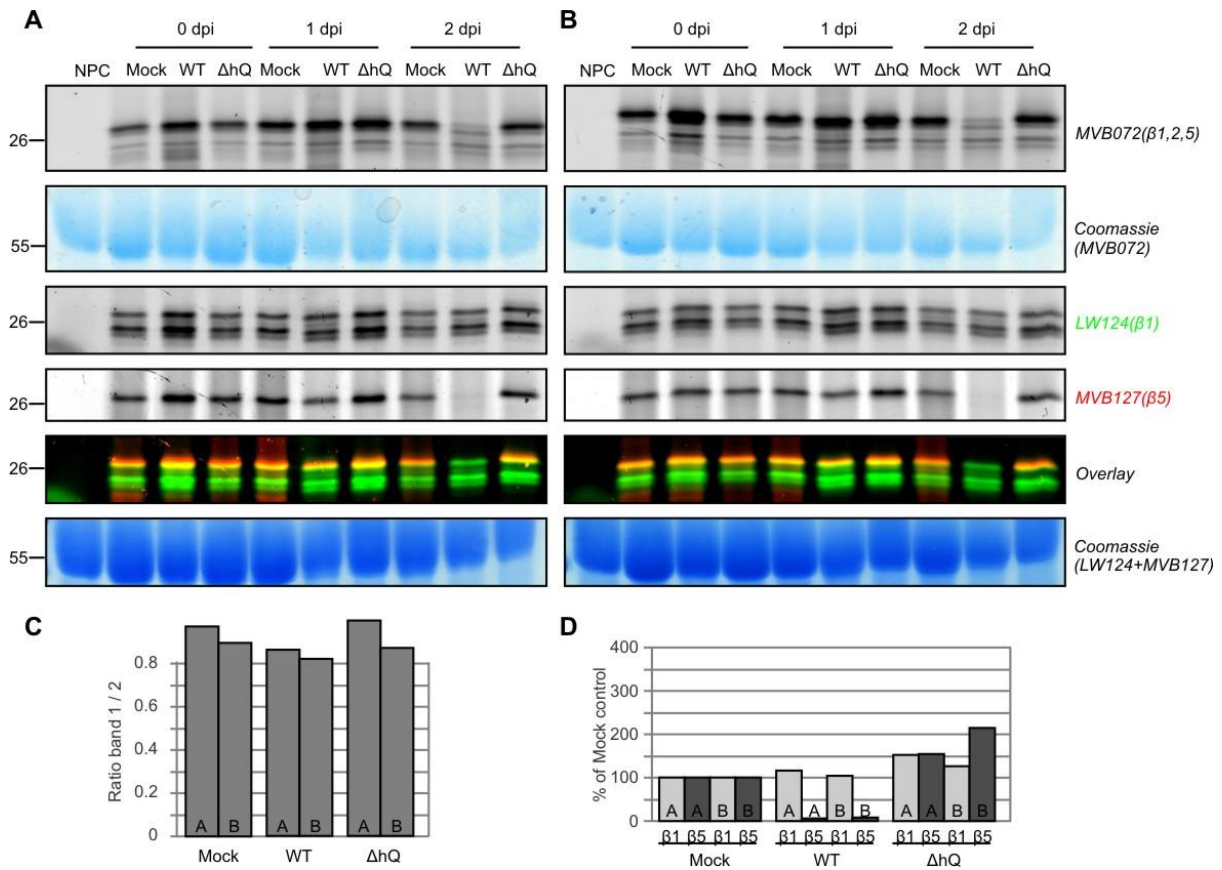
876

877 **Figure S5.** Increased proteasome activity upon WT infection. Shown is one experiment

878 containing four biological replicates. See **Figure 6** for more details.

879





880

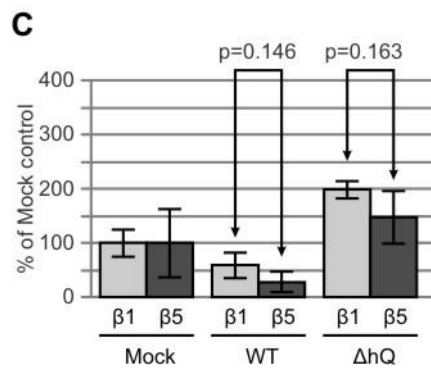
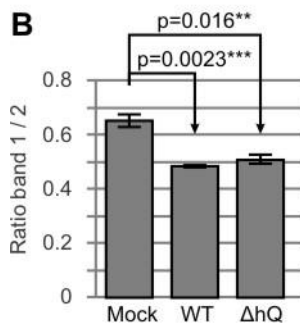
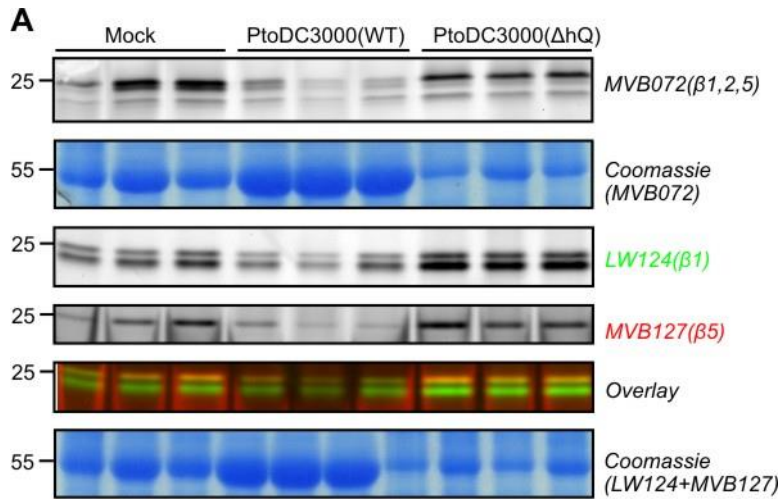
881

882

883

884

**Figure S6.** Suppressed β5 labeling upon WT infection. **A, B**) Shown is one experiment containing two biological replicates. Part of the right half of this figure is shown in **Figure 6bd**. **C**) Ratio of the two β1 signals. **D**) Fluorescent intensity of the signals, normalized to the Mock control. See Figure 6 for more details.



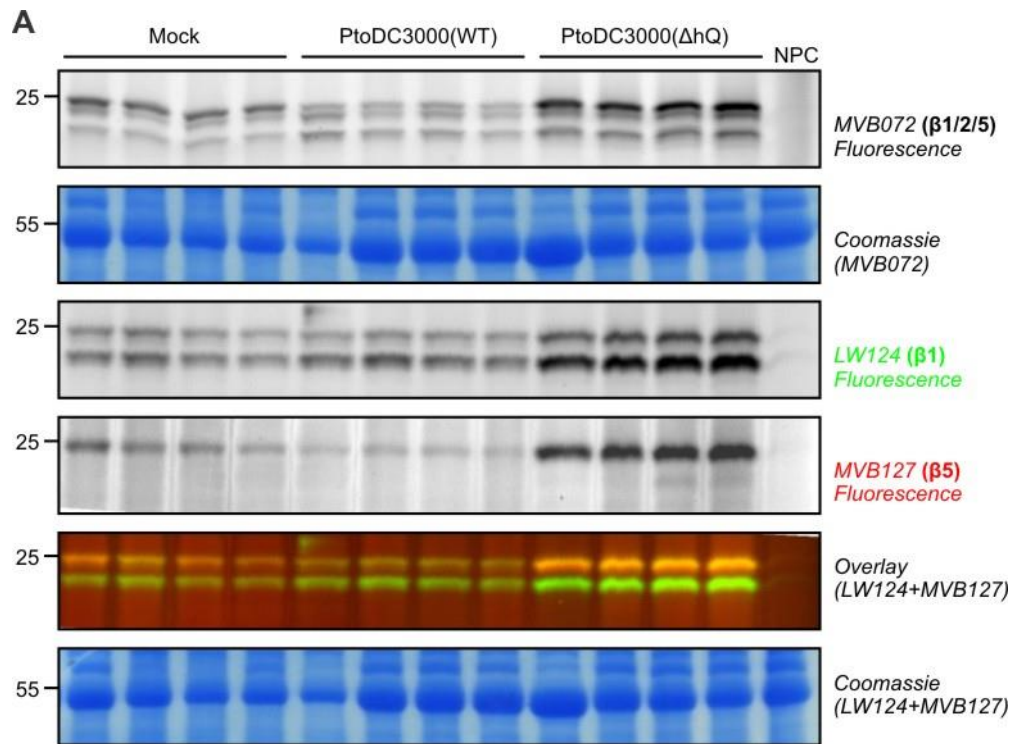
885

886

887

888

**Figure S7.** Suppressed β5 labeling upon WT infection. Shown is one experiment containing three biological replicates. **B)** Ratio of the two β1 signals. **C)** Fluorescent intensity of the signals, normalized to the Mock control. See Figure 6 for more details.

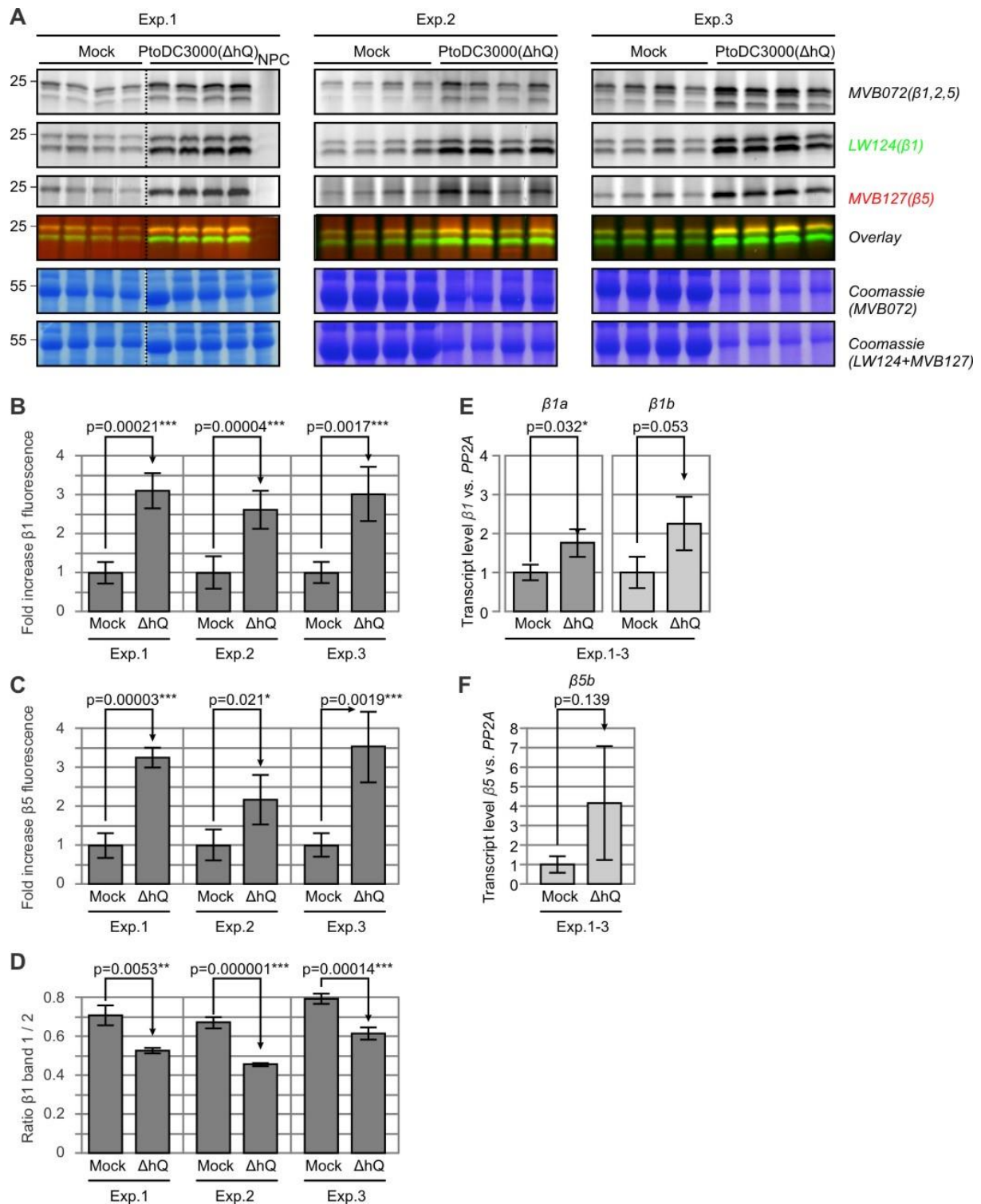


889

890 **Figure S8.** Suppressed  $\beta$ 5 labeling upon WT infection. Shown is one experiment containing four

891 biological replicates. **B)** Ratio of the two  $\beta$ 1 signals. **C)** Fluorescent intensity of the signals,

892 normalized to the Mock control. See Figure 6 for more details.



893

894

895

896

897

898

899

900

**Figure S9** Altered proteasome activity upon infection with PtoDC3000(ΔhQ). **A**) Shown are three independent experiments, each containing four biological replicates. **B, C**) Fluorescence intensity normalized to the Mock control for each of the three experiments. **D**) Ratio of β1 signals 1 and 2 for each of the three experiments. **E, F**) qRT-PCR, performed on the three biological experiments. Replicates of each biological experiment were mixed (n=4) and the average of expression and standard deviation were calculated for the three biological experiments. See **Figure 6** for more details.

901 **Table S1:** Identified peptides of catalytic subunits\*.

Peptide sequence	u/s	score	protein	BTH		H2O	
				MS1	MS2	MS1	MS1
EGMTQEAEAK	s	175.5	beta 1	2	2	2	2
FYPGDSLQLWHEELEPVNSLLDVVSASSPDPMVS	s	110.2	beta 1	1	0	2	0
ITQLTDNVVYVCR	s	283.5	beta 1	4	3	4	4
IYGIPLGGTVLEQPPFAIGGSGSSYLYGFFDQAWK	s	155.5	beta 1	2	1	2	1
KFYPGDSLQLWHEELEPVNSLLDVVSASSPDPMVS	s	57.14	beta 1	1	0	2	0
LLSYNNK	s	128.5	beta 1	1	1	1	1
LQTGMIIIGGWDK	s	151.7	beta 1	3	2	3	3
LVVTAVSLAIAR	s	168.0	beta 1	3	2	2	2
SGSAADSQIVSDYVR	s	254.9	beta 1	2	3	3	1
SGSAADSQVVS DYVR	s	299.2	beta 1	2	2	2	2
TSTGMIVANR	s	228.2	beta 1	5	5	6	5
VAANLVR	s	137.8	beta 1	1	1	1	1
YFLHQHTIQLGQPATVK	s	298.1	beta 1	3	4	4	3
ATEGPIVADK	s	199.3	beta 2	2	3	2	2
ATEGPIVADKNCEK	s	177.0	beta 2	0	0	1	0
GNTEYLR	s	129.7	beta 2	1	1	1	1
IHYMAPNIYCCGAGTAADTEAVTDMVSSQLK	s	138.4	beta 2	1	0	3	0
IIEINPYMLGTMAGGAADCQFWHR	s	103.6	beta 2	2	1	3	0
AIYHATFR	s	204.8	beta 5	1	0	1	0
ASMGYISSQSVK	s	214.6	beta 5	6	4	4	5
DGASGGVASVYHVGPNGWK	s	287.0	beta 5	4	2	4	2
FDLSVEEAAELAR	s	373.7	beta 5	3	4	2	3
FSVSGSPYAYGVLD SGYR	s	242.7	beta 5	4	5	6	5
GGVMVAADSR	s	123.0	beta 5	3	3	3	5
GMGLSVGTMIAGWDEK	s	214.9	beta 5	7	4	8	6
GPGLYYV DSEGGR	s	136.9	beta 5	1	1	2	2
ISVAGASK	s	124.1	beta 5	0	0	1	0
KLSGDDV GELHYNYYPVELESVEQEMAEVPVA	s	57.9	beta 5	2	0	2	0
LHELANK	s	141.0	beta 5	2	1	1	1
LHELANKR	s	141.5	beta 5	1	1	1	0
LLANILYSYR	s	190.6	beta 5	1	1	1	2
LSGDDV GELHYNYYPVELESVEQEMAEVPVA	s	68.84	beta 5	2	2	4	2
RAIYHATFR	s	128.5	beta 5	1	0	1	0
RISVAGASK	s	120.6	beta 5	0	0	1	0
ITQLDNDNVVYVCR	u	218.0	Nbs00001896g0032.1	1	1	2	1
KLSGDDV GELHYSYYPVELESVEQEMAEVPVA	u	50.03	Nbs00002652g0001.1	0	0	1	0
IYGVPLGGTLLEQPPFAIGGSGSSYLYGFFDQAWR	u	111.2	Nbs00009991g0103.1	0	1	0	1
ERVEIEGGDAMEE	u	197.1	Nbs00015516g0007.1	1	0	1	0
NHMLPNPR	u	94.16	Nbs00015516g0007.1	1	0	1	0
LVAEAILSGVFNDLGSGSNVDICITK	u	112.5	Nbs00015516g0007.1	1	1	0	0
VEVIEGGDAMEE	u	202.0	Nbs00015516g0007.1	1	0	1	0
KTEVLLTK	u	181.5	Nbs00022575g0009.1	2	1	2	1
EIVQVIEGGDAMEE	u	227.6	Nbs00022575g0009.1	5	1	4	1
LVAEAILSGVFNDLGSGSNVDICVITK	u	119.2	Nbs00022575g0009.1	1	1	1	0
TEVLLTK	u	143.6	Nbs00022575g0009.1	2	1	2	1

902 \*, unique (u) or shared (s); highest peptide score; protein hit; spectral counts in the two pull down  
903 experiments, each analyzed twice by MS.